Title

Differentiation into an Effector Memory Phenotype Potentiates HIV-1 Latency Reversal in CD4+ T Cells

Journal

Journal of Virology, 93(24)

ISSN

0022-538X

Authors

Kulpa, Deanna A
Talla, Aarthi
Brehm, Jessica H
et al.

Publication Date

2019-12-01

DOI

10.1128/jvi.00969-19

Peer reviewed

AMERICAN SOCIETY FOR MICROBIOLOGY | Journal of Virology®

GENOME REPLICATION AND REGULATION OF VIRAL GENE EXPRESSION

Differentiation into an Effector Memory Phenotype Potentiates HIV-1 Latency Reversal in CD4$^+$ T Cells

Deanna A. Kulpa,[a] Aarthi Talla,[b] Jessica H. Brehm,[c] Susan Pereira Ribeiro,[b] Sally Yuan,[d] Anne-Gaelle Bebin-Blackwell,[e] Michael Miller,[f] Richard Barnard,[f] Steven G. Deeks,[g] Daria Hazuda,[f] Nicolas Chomont,[h,i] Rafick-Pierre Sékaly[b]

[a]Department of Pediatrics, Emory University, Atlanta, Georgia, USA
[b]Department of Pathology, Case Western Reserve University, Cleveland, Ohio, USA
[c]ViiV Healthcare, Research Triangle Park, North Carolina, USA
[d]Janssen Pharmaceuticals, Springhouse, Pennsylvania, USA
[e]University of Georgia, Athens, Georgia, USA
[f]Infectious Disease, Merck & Co., Inc., West Point, Pennsylvania, USA
[g]Department of Medicine, University of California, San Francisco, San Francisco, California, USA
[h]Centre de Recherche du CHUM, Montréal, Quebec, Canada
[i]Université de Montréal, Department of Microbiology, Infectiology, and Immunology, Montréal, Quebec, Canada

ABSTRACT During antiretroviral therapy (ART), human immunodeficiency virus type 1 (HIV-1) persists as a latent reservoir in CD4$^+$ T cell subsets in central memory (T_{CM}), transitional memory (T_{TM}), and effector memory (T_{EM}) CD4$^+$ T cells. We have identified differences in mechanisms underlying latency and responses to latency-reversing agents (LRAs) in *ex vivo* CD4$^+$ memory T cells from virally suppressed HIV-infected individuals and in an *in vitro* primary cell model of HIV-1 latency. Our *ex vivo* and *in vitro* results demonstrate the association of transcriptional pathways of T cell differentiation, acquisition of effector function, and cell cycle entry in response to LRAs. Analyses of memory cell subsets showed that effector memory pathways and cell surface markers of activation and proliferation in the T_{EM} subset are predictive of higher frequencies of cells carrying an inducible reservoir. Transcriptional profiling also demonstrated that the epigenetic machinery (known to control latency and reactivation) in the T_{EM} subset is associated with frequencies of cells with HIV-integrated DNA and inducible HIV multispliced RNA. T_{CM} cells were triggered to differentiate into T_{EM} cells when they were exposed to LRAs, and this increase of T_{EM} subset frequencies upon LRA stimulation was positively associated with higher numbers of p24$^+$ cells. Together, these data highlight differences in underlying biological latency control in different memory CD4$^+$ T cell subsets which harbor latent HIV *in vivo* and support a role for differentiation into a T_{EM} phenotype in facilitating latency reversal.

IMPORTANCE By performing phenotypic analysis of latency reversal in CD4$^+$ T cells from virally suppressed individuals, we identify the T_{EM} subset as the largest contributor to the inducible HIV reservoir. Differential responses of memory CD4$^+$ T cell subsets to latency-reversing agents (LRAs) demonstrate that HIV gene expression is associated with heightened expression of transcriptional pathways associated with differentiation, acquisition of effector function, and cell cycle entry. *In vitro* modeling of the latent HIV reservoir in memory CD4$^+$ T cell subsets identify LRAs that reverse latency with ranges of efficiency and specificity. We found that therapeutic induction of latency reversal is associated with upregulation of identical sets of T_{EM}-associated genes and cell surface markers shown to be associated with latency reversal in our *ex vivo* and *in vitro* models. Together, these data support the idea that the effector memory phenotype supports HIV latency reversal in CD4$^+$ T cells.

Citation Kulpa DA, Talla A, Brehm JH, Ribeiro SP, Yuan S, Bebin-Blackwell A-G, Miller M, Barnard R, Deeks SG, Hazuda D, Chomont N, Sékaly R-P. 2019. Differentiation into an effector memory phenotype potentiates HIV-1 latency reversal in CD4$^+$ T cells. J Virol 93:e00969-19. https://doi.org/10.1128/JVI.00969-19.

Editor Viviana Simon, Icahn School of Medicine at Mount Sinai

Address correspondence to Deanna A. Kulpa, deanna.kulpa@emory.edu, or Rafick-Pierre Sékaly, rafick.sekaly@case.edu.

Received 10 June 2019
Accepted 15 September 2019
Accepted manuscript posted online 2 October 2019
Published 26 November 2019

KEYWORDS CD4 T cells, HIV latency, HIV persistence

The lifelong persistence of latently infected cells is a major obstacle toward human immunodeficiency virus type 1 (HIV-1) eradication in individuals on long-term antiretroviral therapy (ART). HIV-1 persists in a variety of different cells, including naive $CD4^+$ T cells and myeloid cells; however, the majority of proviral HIV-1 DNA is found in $CD4^+$ T cells displaying a memory phenotype (1–6). Memory $CD4^+$ T cells, such as central memory (T_{CM}), transitional memory (T_{TM}), and effector memory (T_{EM}) $CD4^+$ T cells, are each endowed with very distinct functional and survival properties; T_{EM} cells rapidly upregulate effector function, and T_{CM} cells preserve immune memory by upregulating pathways that aid in long-term (years to decades) survival (3, 4). T_{CM} cells express the costimulatory molecule CD27 (7) as well as CD62L and CCR7, two surface molecules that facilitate migration to T cell zones within lymph nodes and mucosal lymphoid organs. T_{CM} cells are characterized by a delay in effector cytokine production (gamma interferon [IFN-γ], tumor necrosis factor alpha [TNF-α]) after T cell receptor (TCR) stimulation; however, they readily proliferate and differentiate into effector cells in response to antigenic stimulation (reviewed in reference 8). T_{CM} cells are more resistant to Fas-induced apoptosis than T_{EM} cells (9–12); their apoptosis is mediated through the activation and phosphorylation of STAT5a and inactivation of the transcriptional repressor FOXO3a (13). In contrast, T_{EM} cells ($CCR7^-$ $CD27^-$) express homing receptors for migration to nonlymphoid sites of inflammation and have high levels of gut-homing molecules ($\alpha_4\beta_7$ integrin) and chemokine receptors that target these cells to nonlymphoid tissues (reviewed in reference 8). T_{CM} and T_{EM} cells are maintained through homeostatic proliferation, although T_{EM} cells show more rapid turnover, indicating that these cells are replaced at a higher rate (14). T_{TM} cells ($CCR7^-$ $CD27^+$) display an intermediate phenotype characterized by lower responsiveness to interleukin 15 (IL-15) than that of T_{EM} cells and transcript expression levels that more closely align with T_{EM} cells for some transcripts (*CD62L*, *TOSO*, and *PIM2*) and with T_{CM} cells for others (*Bim*, *FasL*, and *IFN-*γ [13, 15–18]). T_{CM} and T_{EM} cells show distinct epigenetic profiles, as T_{EM} cells are poised to respond to antigen and quickly produce effector cytokines, whereas T_{CM} cells are quiescent cells that require strong stimulation and costimulation to respond to their cognate antigen (19, 20). Significantly, all memory $CD4^+$ T cell subsets have been shown to contribute to HIV persistence and harbor replication-competent HIV-1 (1, 3–5, 21–23), but recent evidence has suggested that T_{EM} cells harbor more intact HIV-1 provirus than either T_{CM} or T_{TM} cells (24). However, the mechanisms responsible for the persistence of the HIV-1 reservoir in these distinct memory $CD4^+$ T cell subsets *in vivo* are still largely unknown, which may be critical for the development of effective eradication strategies.

One eradication strategy, the "shock and kill" approach, aims to eliminate the HIV-1 reservoir through latency reversal and immunological clearance (25). Given the inherent molecular differences that define the biology of T_{CM}, T_{TM}, and T_{EM} cells, it is unclear whether the same interventions will be equally effective in these distinct populations. Theoretically, the different activation states and basal expression levels of transcription factors within these subsets might affect the activity of latency-reversing agents (LRAs). Here, we examine the impact of the memory $CD4^+$ T cell subset phenotype on HIV-1 latency reversal. We show in *ex vivo* and *in vitro* models that the differentiated phenotype of T_{EM} cells from that of quiescent T_{CM} cells is associated with a brisker response to LRAs, suggesting that differentiation of latently infected cells into T_{EM} cells may facilitate their elimination in the context of a shock and kill approach.

RESULTS

The T_{EM} subset shows the highest levels of the inducible HIV reservoir. The diversity of transcriptional and functional programs of memory $CD4^+$ T subsets (3, 4, 7–14) led us to hypothesize that the subsets show varied capacities to support HIV-1 latency reversal. We characterized T_{CM}, T_{TM}, and T_{EM} cells from two cohorts of virally

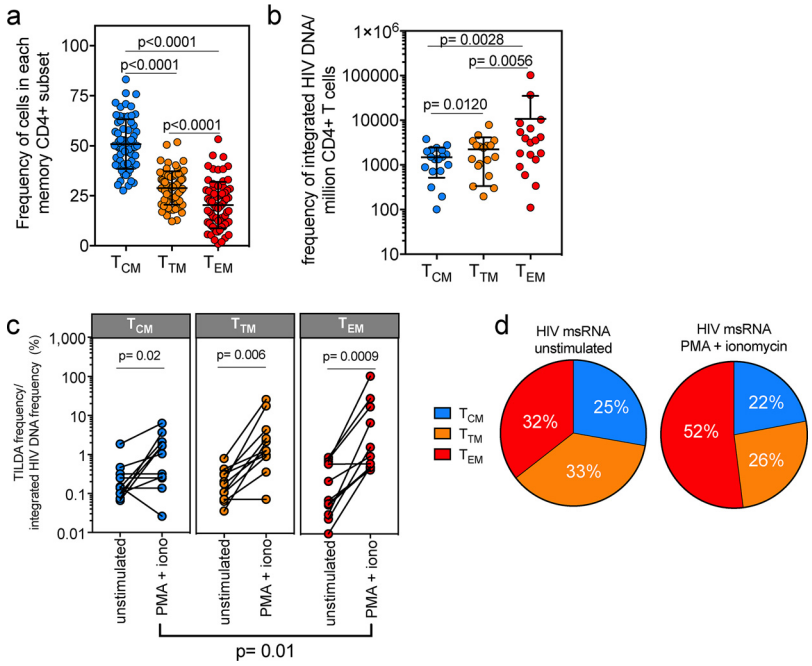

FIG 1 The inducible HIV reservoir resides in the T_{EM} subset. (a) The distribution of the T_{CM}, T_{TM}, and T_{EM} subsets in *ex vivo* memory $CD4^+$ T cells is shown, and *P* values are indicated. Each circle represents individual participants from Table S1 in the supplemental material (bars indicate means with standard deviations [SD], Wilcoxon matched-pair signed-rank test, $n = 69$). (b) $CD4^+$ T cells from virally suppressed individuals were sorted into T_{CM}, T_{TM}, and T_{EM} subsets using the gating strategy in Fig. S1 in the supplemental material, and integrated HIV DNA in each subset was quantified. Bars indicate means with SD from a Wilcoxon matched-pair signed-rank test; *P* values are indicated ($n = 18$). (c) The frequency of transcription of HIV msRNA induced by PMA plus ionomycin (iono), normalized by the amount of integrated HIV DNA in each subset, is shown. Unstimulated sorted subsets were included as a control. There was no statistical difference between levels of HIV msRNA in cells from the $CD4^+$ memory subsets before activation. After exposure to PMA and ionomycin, the frequency of HIV msRNA was quantified and calculated. *P* values are indicated. (Wilcoxon matched-pair signed-rank test; $n = 11$). (d) Contribution of HIV msRNA from each $CD4^+$ memory subset from panel c. All undetectable values were input as zero. The contributions of the T_{CM}, T_{TM}, and T_{EM} subsets to the overall HIV msRNA signal are shown. Each pie slice was calculated using the frequency of HIV msRNA in each memory subset as a percentage of the total signal. Frequency is indicated within each pie slice ($n = 11$).

suppressed individuals, one from San Francisco, CA (Study of the Consequences of the Protease Inhibitor Era [SCOPE] cohort; $n = 47$), and the other from Fort Pierce, FL (FL cohort; $n = 22$) (see Table S1 in the supplemental material). From peripheral blood mononuclear cells (PBMCs) from these two cohorts, we measured the memory cell subset frequencies in each participant and identified the T_{CM} subset to be the most prevalent in memory ($CD45RA^-$) $CD4^+$ T cells (mean, 51%; $P < 0.0001$) (Fig. 1a; Fig. S1a) compared to the T_{TM} and T_{EM} subsets (means, 29% and 20%, respectively). We obtained apheresis products from 18 participants from the FL cohort in order to sort *ex vivo* T_{CM}, T_{TM}, and T_{EM} cells and then identified the T_{EM} subset to have the highest frequency of integrated HIV DNA (Fig. 1b) (26). After normalization to the proportion of cells in each subset, there was no difference in the contributions of the subsets to the reservoir (Fig. S1b). To determine the size of the inducible reservoir in each memory $CD4^+$ T cell subset, we used the *Tat*/*rev*-induced limiting dilution assay (TILDA), which quantifies the frequency of cells induced to express HIV multiply spliced RNA (HIV msRNA) after phorbol myristate acetate (PMA) plus ionomycin treatment (27). Eleven participants from the FL cohort were then selected to represent the range of integrated HIV DNA frequencies that we found within in each subset (Fig. S1c), and TILDA was performed on sorted T_{CM}, T_{TM}, and T_{EM} cell populations (Fig. 1c). After normalization of inducible HIV msRNA expression to the frequency of integrated HIV DNA within each subset, we determined that the T_{EM} subset encompassed higher frequencies of cells with inducible

genomes than the T_{CM} subset ($P = 0.01$; median for T_{EM} cells = 22-fold, median for T_{TM} cells = 8-fold, median for T_{CM} cells = 3-fold) (Fig. 1c) and also was the largest contributor to the pool of cells producing HIV msRNA (Fig. 1d). These data show that although all memory $CD4^+$ T cell subsets contribute to HIV persistence (1), the T_{EM} subset shows the highest frequency of cells with an inducible reservoir.

Effector T cell differentiation and cell cycle entry transcriptional programs are associated with HIV reactivation. Based on these data, we used a transcriptomics approach to test the hypothesis that a T_{EM} cell-specific gene signature supported HIV expression at a higher frequency than that of a T_{CM} cell. We initially assessed the correlation between pathways and HIV expression in *ex vivo*-sorted memory $CD4^+$ T cell subsets from nine FL cohort participants that represented the range of TILDA frequencies measured in Fig. 1c (T_{CM} cell range in TILDA values, 1.1 to 85; T_{EM} cell range in TILDA values, 5.6 to 2,506). Results illustrated in Fig. 2a demonstrate that cell cycling expression (targets of E2F transcription factors) and targets of NF-κB expressed *ex vivo* significantly correlated with the frequency of the inducible reservoir in T_{CM} or T_{EM} cells (P value < 0.001, rho = 0.8) and that these pathways were preferentially expressed more highly in the T_{EM} cells (P value = 0.003), highlighting the importance of proliferation and NF-κB (known to enhance viral replication) in the capacity to respond to PMA plus ionomycin activation. Memory $CD4^+$ T cell subsets from five participants from the FL cohort were further assessed for responses to LRAs. We quantified HIV msRNA from sorted memory subsets that had been exposed to three distinct LRAs, the protein kinase C (PKC) agonist bryostatin, the γ-chain cytokine IL-15, or PMA plus ionomycin. T_{EM} cells again showed significant induction of HIV msRNA expression, with a mean 35-fold increase ($P = 0.01$) (Fig. 2b) compared to its expression in other subsets. Transcriptional profiling was then used to identify mechanisms specific to T_{CM}, T_{TM}, and T_{EM} cells associated with LRA responses in three out of the five participants. First, we confirmed that T_{EM} cells intrinsically (prestimulation) showed higher expression of pathways and genes associated with effector function, cell cycle progression, and HIV RNA transcription and replication than T_{CM} cells (Fig. 2c; Table S2) (28). Here, the *ex vivo* T_{CM} cells showed higher expression of quiescence signatures, such as epigenetic repressors (HDAC1 and NCOR2) and genes downstream of the TGF-β signaling pathway (ACVR1, FNTA, LTBP2) (Fig. 2c, Table S2) (29). However, after bryostatin stimulation, the T_{CM} subset was induced to express genes involved in effector function, cell cycling, and HIV transcription, indicating that the exposure of T_{CM} cells to LRAs triggered the expression of pathways and genes which are hallmarks of T_{EM} cells (Fig. 2d). Hierarchical clustering of these pathways showed that the bryostatin-stimulated T_{CM} subset exhibited pathway expression profiles similar to those of the unstimulated T_{EM} subset (Fig. 2e). Transcriptional profiles of the T_{CM} subset exposed to PMA plus ionomycin activation also showed gene and pathway similarity to those of unstimulated T_{EM} cells (Fig. S2a).

The pathways modulated in T_{CM} cells upon exposure to bryostatin or PMA plus ionomycin included genes encoding several cytokines with effector functions (gamma interferon [IFN-γ], IL-2, IL-9, tumor necrosis factor alpha [TNF-α], granzyme A [GZMA]) as well as activation markers (CD38, CD69, CD25 IL2RA) (Fig. 2f and g; Table S3). Importantly, T_{CM} cells upregulated the expression of transcription factors known to activate HIV-1 transcription; these factors included NFAT5, STAT5, NF-κB, E2F, and their targets, i.e., topoisomerase 2A (TOP2A) (30–32) and the eukaryotic translation apparatus (EIF2S1, EIF4A1) (33). The PKC activation pathway, known to facilitate HIV-1 latency reversal by triggering NF-κB (34–36), was also upregulated in T_{CM} cells exposed to PMA plus ionomycin (Fig. 2g). These effector pathways also were all upregulated in T_{EM} cells upon exposure to LRAs, including the kinase PIM-1 (37), a major contributor to HIV-1 reactivation (Fig. S2b; Table S4).

Significantly, bryostatin downregulated FOXO1 and its targets (a transcriptional regulator that controls the differentiation of T_{CM} cells [38–41]) in T_{CM} cells (Fig. 2f). These included the FOXO1 gene and genes like the transcription factor that controls the maintenance of the memory T cell stem cell program TCF7, the cell cycle inhibitor

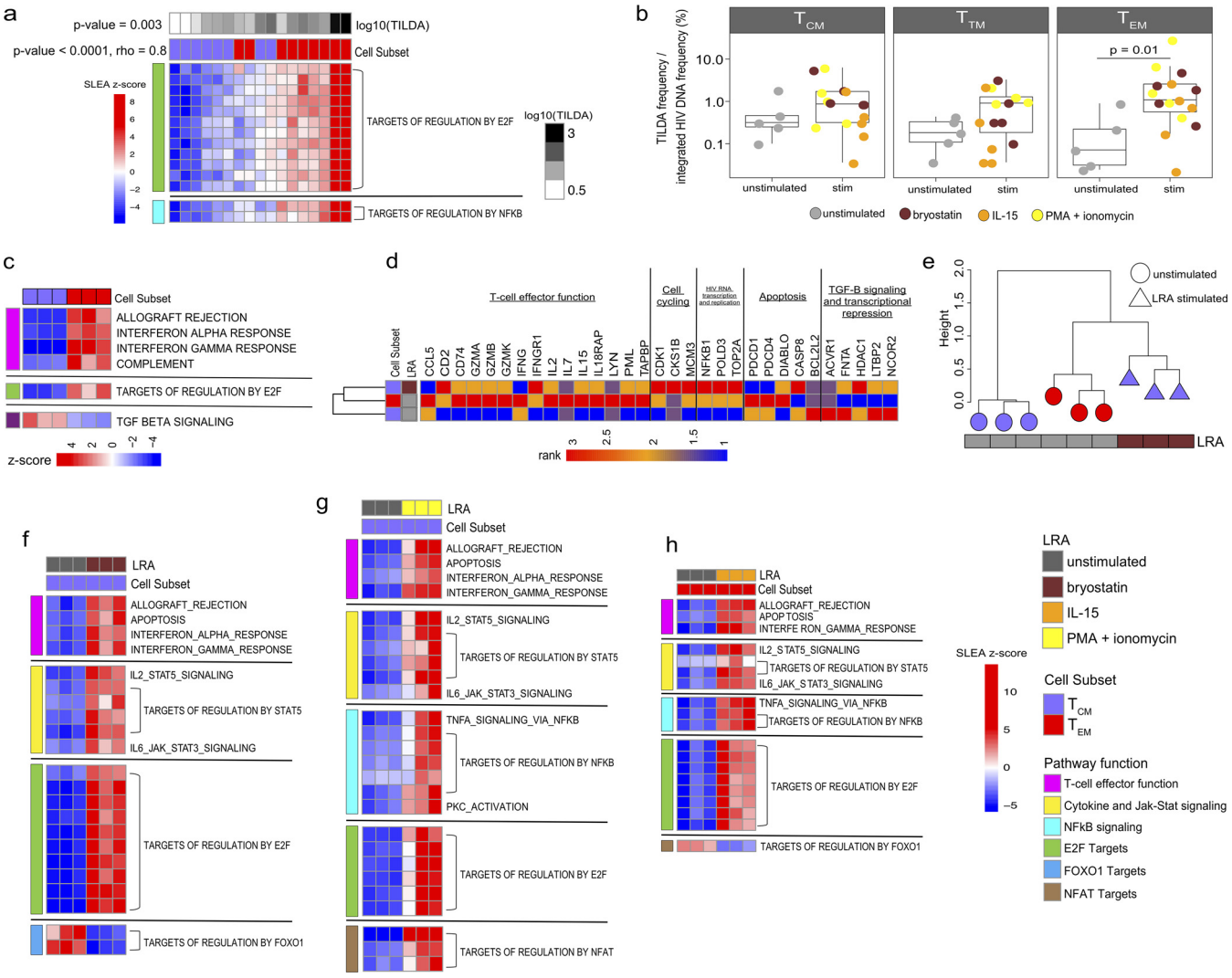

FIG 2 Latency reversal is associated with the upregulation of T cell effector pathways. (a) Heatmap of the gene sets expressed in sorted *ex vivo* T_{EM} and T_{CM} cells from the FL cohort correlated with the frequency of cells expressing HIV msRNA measured by TILDA ($n = 9$). GSEA was first performed to identify pathways/gene sets correlated with TILDA across the cell subsets, and then the SLEA z-score of the pathway was calculated per sample, represented by the color gradient. Rows represent the pathway, and columns represent samples. Samples were ordered by increasing expression of the pathway associated with TILDA (mean rank ordering). The association between the mean rank and TILDA is then tested with a Spearman correlation, and its *P* value and rho are indicated next to the TILDA annotation bar. The increasing pathway expression is associated with increasing TILDA values (*P* value < 0.0001, rho $= 0.8$). A Wilcox test is then performed to assess the difference in mean ranks between T_{EM} and T_{CM} cells. The Wilcox test *P* value is then indicated next to the cell subset annotation bar. These gene sets also show higher expression in T_{EM} cells than in T_{CM} cells (*P* value $= 0.003$). (b) We examined the inducible reservoir in sorted memory $CD4^+$ T cell subsets from virally suppressed HIV-infected individuals (FL cohort; $n = 5$). Sorted memory $CD4^+$ T_{CM}, T_{TM}, and T_{EM} subsets were exposed to 100 ng/ml PMA plus 1 μg/ml ionomycin, 10 ng/ml IL-15, or 10 nM bryostatin, and the induction of HIV msRNA was measured using TILDA (stimulated [stim]). Untreated cells were used as a control (unstim). The T_{EM} and T_{TM} subsets showed significant induction of HIV msRNA upon stimulation compared to that of the unstimulated controls (Wilcoxon rank sum test; *P* values are indicated). The line in each box plot denotes a median value with SD. (c) Heatmap of the pathways differentially expressed between unstimulated (baseline) $CD4^+$ memory subsets (*P* value < 0.05) from three out of the five individuals shown in panel b. Rows represent the pathway, and columns represent samples. The color gradient represents the z-score of the pathway per sample calculated by SLEA. Effector function and cell cycling pathways show significant upregulation in the T_{EM} subset compared to in the T_{CM} and T_{TM} subsets, while the senescent TGF-β signaling pathway is significantly upregulated in the T_{CM} subset. (d) Heatmap of the genes upregulated in the unstimulated T_{EM} subset compared to those of the unstimulated T_{CM} subset. The average gene expression across the three participants (shown in panel b) per memory subset is shown here. The expression of these genes was also assessed in the bryostatin-stimulated T_{CM} cells, showing that the stimulated T_{CM} cells have a gene expression profile similar to that of the unstimulated T_{EM} cells. The color gradient represents the rank of the gene expression across subsets ($n = 3$). (e) Hierarchical clustering on the pathways in the T_{CM} subset upon exposure to bryostatin that was differentially expressed from that of the unstimulated controls (*P* value < 0.05). The pathway expression was assessed in the T_{CM} subset and in the unstimulated T_{EM} subset. Similarities in gene expression were determined using the complete linkage clustering method, with the distance between gene expression profiles measured using Euclidean distance. The height of a dendrogram represents the Euclidean distance. The bryostatin-stimulated T_{CM} subset is in close proximity to the unstimulated T_{EM} subset. (f and g) Heatmap of the pathways in the T_{CM} subset upon exposure to LRAs (bryostatin [e] or PMA plus ionomycin [f]) that were differentially expressed from those of their unstimulated controls (*P* value < 0.05). Rows represent the pathway, and columns represent samples. The color gradient represents the z-scores of the pathway per sample calculated by SLEA. Pathways are grouped by biological function. (h) Heatmap of the pathways differentially expressed in the T_{EM} subset upon exposure to IL-15 (*P* value < 0.05).

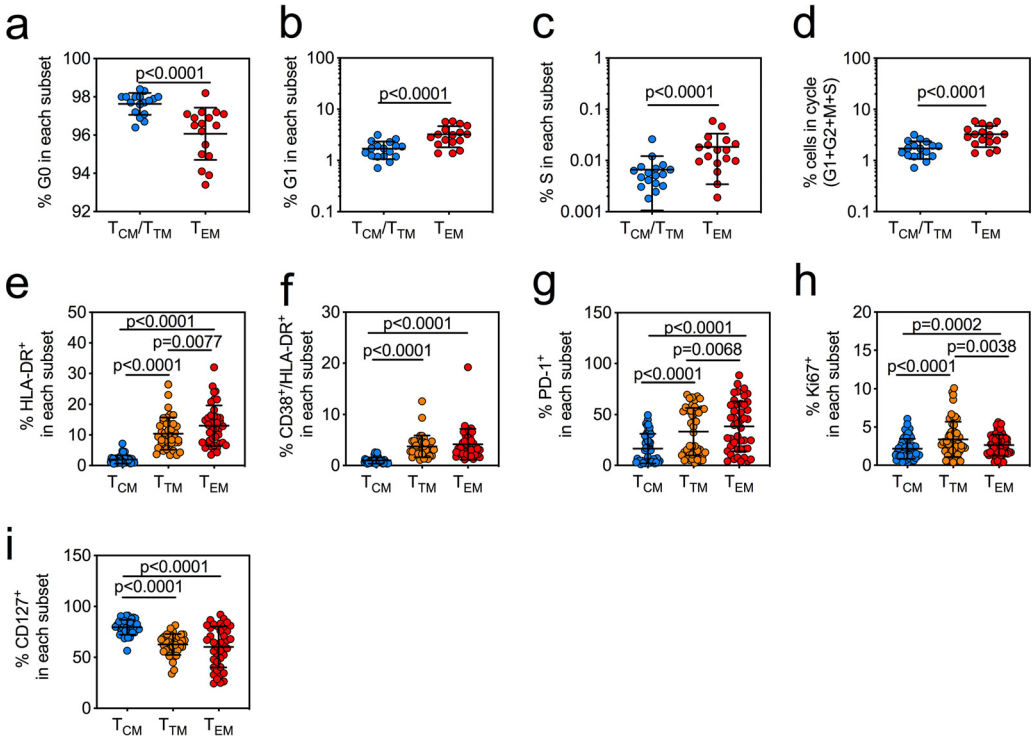

FIG 3 The T_{EM} subset is characterized by expression of markers of cell cycle entry and of T cell activation. (a to c) Percentages of $CD4^+$ T cells in the T_{CM}/T_{TM} subsets (blue circles) and T_{EM} subsets (red circles) in resting phase (G_0) (a), growth phase (G_1) (b), and DNA synthesis phase (S) and mitosis phase (M) (c) of the cell cycle from virally suppressed HIV-infected individuals (bars indicate means with SD from a Wilcoxon matched-pair signed-rank test [$n = 17$]). (d) Percentages of cells in the cycle are represented with the equation $[(G_1 + G_2 + M + S)/(G_0 + G_1 + G_2 + M + S)] \times 100$, which shows significantly more cycling cells in the T_{EM} subset than in other subsets (bars indicate means with SD from a Wilcoxon matched-pair signed-rank test [$n = 17$]). (e to i) Percentages of cells in the T_{CM} (blue circles), T_{TM} (orange circles), and T_{EM} (red circles) subsets positive for HLA-DR ($n = 45$) (e) or coexpressing CD38/HLA-DR ($n = 45$) (f), PD-1 ($n = 45$) (g), Ki67 ($n = 57$) (h), or CD127 ($n = 40$) (i). *P* values are indicated from a Mann-Whitney test. Measurements were based upon the availability of cells from each cohort.

CDKN1A, the chromatin-remodeling protein ARID4A, which recruits histone deacetylases (HDACs) to silence HIV-1, the transcriptional repressor MAFF, and the BCL2 family gene *BMF*. In T_{EM} cells, bryostatin-downregulated FOXO1 targets included RUNX1, known to bind the HIV long terminal repeat (LTR) and to repress transcription (42), and BMF (Fig. 2f; Fig. S2b; Table S3; Table S4). Both ID2 and IRF4, factors critical for promoting the differentiation of T_{CM} to T_{EM} cells, were upregulated in T_{CM} and T_{EM} cells upon exposure to bryostatin and/or PMA plus ionomycin (Table S3; Table S4) (43, 44; unpublished data). In addition, the upregulation of these effector pathways and downregulation of FOXO1 and its targets were also observed specifically in the T_{EM} subset upon stimulation with IL-15 (Fig. 2h). PMA plus ionomycin stimulation of T_{TM} cells also triggered the upregulation of the above-mentioned pathways, all of which overlapped those expressed by T_{CM} and T_{EM} cells (Fig. S2c; Table S3).

Markers of T cell activation predict the inducible HIV reservoir in memory subsets. Transcriptional profiling showed that LRAs triggered the expression of genes associated with T cell activation and cell cycle entry (Fig. 2c to h). To determine if expression of these pathways *ex vivo* correlated with the frequency of cells that harbor inducible HIV, we quantified T_{CM}, T_{TM}, and T_{EM} cells for cell cycle frequency and activation marker expression in cells from the SCOPE and FL cohorts from Fig. 1 (Fig. 3). We quantified the proportions of *ex vivo* $CD4^+$ T cells from virally suppressed HIV-infected individuals in resting (G_0) or active (G_1, S, and G_2M) cells and found that T_{EM} cells had significantly higher frequencies of cells progressing through the cell cycle ($P < 0.0001$) (Fig. 3a to d). T_{TM} and T_{EM} cells also had significantly higher frequencies of the activation and proliferation markers HLA-DR ($P < 0.0001$), CD38 ($P < 0.0001$), PD-1

TABLE 1 Activation markers expressed in T_{CM} and T_{EM} cells that best predicted the frequency of cells expressing inducible HIV msRNA[a]

Subset	Activation marker	Coefficient
T_{CM} cells	Ki67	0.5
	HLADR	–0.1
	PD-1	–0.8
T_{EM} cells	PD-1	0.03
	CD127	0.2
	Ki67	0.6
	HLADR/CD38	–0.3

[a]A LASSO regression model was built with the activation markers as independent variables and the frequency of cells expressing inducible HIV msRNA as the dependent variable. The models were optimized via leave-one-out cross-validation, and the least cross-validated mean square error was determined. The regression coefficient for each marker is provided.

($P < 0.0001$), and Ki67 ($P < 0.0001$, $P = 0.0002$), while T_{CM} cells maintained the highest levels of CD127 (IL-7Rα) ($P < 0.0001$) (Fig. 3e to i). CD127 expression is associated with a greater ability to become a long-term memory cell and indicates dependence on IL-7 signals for homeostatic maintenance (45–50). We then used an unbiased least absolute shrinkage and selection operator (LASSO) regression analysis (51) to identify the cell surface markers of T cell activation expressed by each memory T cell subset *ex vivo* that best predicted the features of a population of cells within each subset that would support an inducible HIV reservoir. These models were optimized via leave-one-out cross-validation, and the model with the least cross-validated mean square error was chosen (0.37 for T_{CM} cells and 0.32 for T_{EM} cells) (Fig. S3a and b). Our data show that the induction of HIV msRNA in *ex vivo* T_{CM} cells was best associated with cells expressing high Ki67, a marker of cell proliferation, and low HLA-DR and PD-1 (Table 1, T_{CM} subset; Fig. S3a), with a cross-validated mean square error close to 0 to 0.3 and an adjusted R^2 of 73%, indicating that these proliferating cells were partially activated and suggesting a response driven by γ-chain cytokines, which we have shown are critical in HIV reservoir maintenance (Table 1, T_{CM} subset) (1). Whereas in the T_{EM} cells, expression of high Ki67, PD-1, and CD127 best predicted frequencies of cells with inducible HIV msRNA (Table 1, T_{EM} subset, and Fig. S3b, with a cross-validated mean square error close to 0 to 0.3 and an adjusted R^2 of 70%). These cells also express low HLA-DR and CD38, supporting previous observations that the reservoir in the T_{EM} subset is maintained in resting populations (52, 53).

We assessed in sorted $CD4^+$ T_{CM} and T_{EM} subsets the enrichment of pathways involved in epigenetic modifications and transcriptional control that include NAD-dependent histone deacetylase (sirtuins) (54, 55), NAD-independent histone deacetylase (56, 57), histone acetyltransferases (HATs) (58–61), and other chromatin-modifying enzymes (SWI/SNF-related, matrix-associated, actin-dependent regulator chromatin group A [SMARCA]) (62–64). Genes that control the establishment of HIV latency (HDACs) (64) as well as epigenetic silencing genes (RUNXs) and SMARCAs, i.e., genes that inhibit the unwinding of chromatin, were all expressed at higher levels in T_{EM} than in T_{CM} cells (Fig. 4). Importantly, heightened expression of these genes was positively correlated with the levels of inducible HIV msRNA as well as with frequencies of cells with integrated HIV DNA (Fig. 4a and b; Table S5). The expression of genes involved in the reactivation of latent HIV, like the HATs KAT2A and KAT5 (65), was higher in the T_{EM} subset and specifically correlated with the highest levels of inducible HIV msRNA (Fig. 4a).

Transcriptional profiling and phenotypic analyses showed that expression of genes, pathways, and cell surface markers involved in T cell activation/proliferation in the T_{EM} subset enhanced the response of this subset to LRAs compared to that of the T_{CM} or T_{TM} subset. The enhanced response of the T_{EM} subset also correlates with chromatin remodeling, such as modulation of histone acetyltransferase and deacetylase enzymes. These data, together with the phenotypic analyses, indicate that distinct mechanisms may regulate HIV latency in different memory $CD4^+$ T cell subsets.

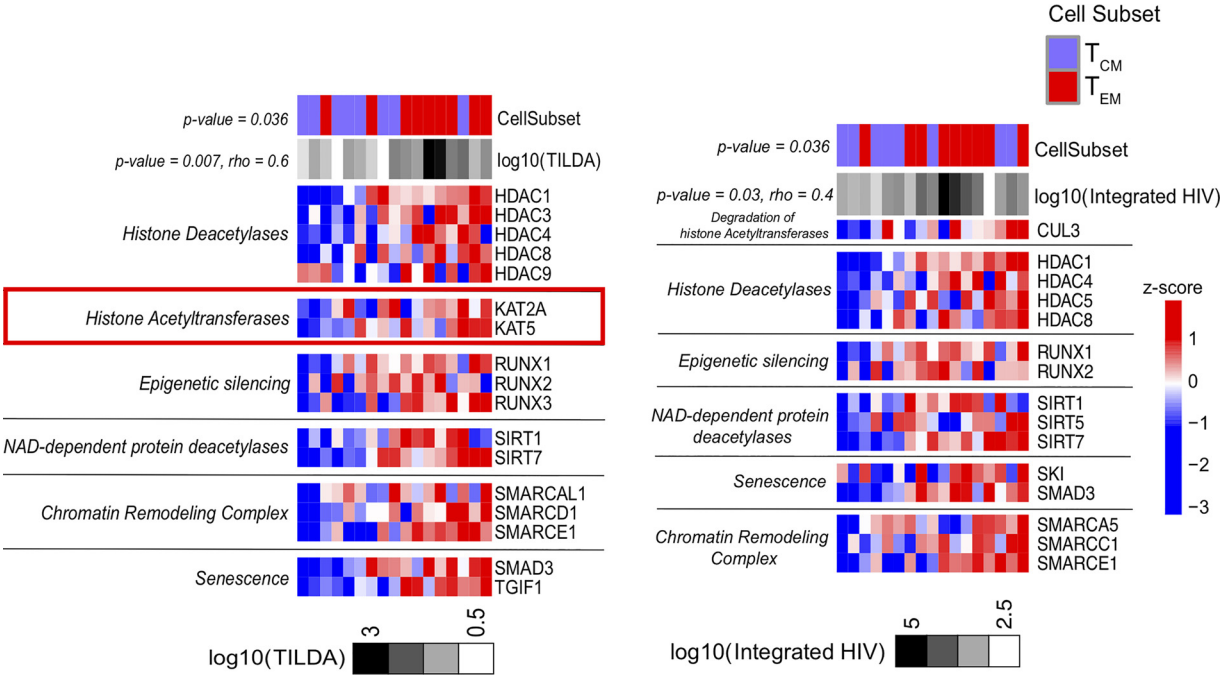

FIG 4 The HDAC pathway expressed in the T_{EM} subset is correlated with the induction of HIV msRNA. Heatmaps of the leading-edge genes, enriched among the genes correlated with the induction of HIV msRNA measured by TILDA (left) and with the levels of integrated HIV DNA on sorted CD4$^+$ T_{CM} and T_{EM} subsets from the Florida cohort (right), by running GSEA using the HDAC pathway gene set from the Pathway Interaction Database (PID; http://pid.nci.nih.gov/) and custom gene sets of chromatin remodeling (PubMed identifier, 29236683) as the database (P value $<$ 0.05). Samples were ordered by increasing the expression of the genes associated with $\log_{10}$(TILDA) or $\log_{10}$(integrated HIV DNA) (mean rank ordering). The association between the mean rank and TILDA result is then tested with a Spearman correlation, and its P value and rho are indicated next to the TILDA result and integrated HIV DNA annotation bar. The increasing gene expression is associated with increasing TILDA values (P value = 0.007, rho = 0.6) and with integrated HIV (P value = 0.03, rho = 0.4). A Wilcox test is then performed to assess the difference in mean ranks between T_{EM} and T_{CM} cells. The Wilcox test P value is then indicated next to the cell subset annotation bar, and these genes show higher expression in T_{EM} than in T_{CM} cells (P value = 0.036).

The LARA recapitulates the complex dynamics of the establishment and maintenance of the latent reservoir in different memory T cell subsets. We developed a latency and reversion assay (LARA), an *in vitro* model, to characterize the mechanisms that trigger HIV latency and reversal in each memory CD4$^+$ T cell subset and confirm our *ex vivo* findings (Fig. 5a). To establish HIV latency *in vitro*, LARA conditions were optimized to mimic the homeostatic T cell environment in lymph nodes, which supports the long-term maintenance of memory CD4$^+$ T cells, including the addition of transforming growth factor β (TGF-β) and IL-7, two cytokines that promote T cell survival and quiescence (29, 66–71), and conditioned medium from the glioblastoma cell line H-80 (72, 73), which also contains cytokines that promote quiescence (TGF-β1, -2, and -3 and IL-9) and survival (IL-21) (Fig. S4a) (74). Phenotypic assessment showed that LARA conditions supported the maintenance *in vitro* of all memory subsets (T_{CM}, T_{TM}, and T_{EM}) as well as functional CD4$^+$ T cell subsets (Th1, Th2, Th17) (Fig. 5b; Fig. S4b). To determine the frequency of infected cells in each memory subset, we sorted LARA T_{CM}, T_{TM}, and T_{EM} cells and quantified integrated HIV DNA (26). After normalizing the frequency of integrated HIV by the proportion of cells in each subset, we demonstrated that LARA culture conditions recapitulated the distribution hierarchy of HIV-infected memory CD4$^+$ T cell subsets similar to those previously observed *in vivo* (1), with the T_{CM} subset contributing the most to the frequency of cells carrying integrated HIV DNA, followed by the T_{TM} and T_{EM} subsets (Fig. 5c).

Transcriptional profiling was performed to confirm that cells in LARA *in vitro* culture maintained the signatures characteristic of *ex vivo* memory subsets. Sorted memory CD4$^+$ T cells that had been cultured in the presence of TGF-β and IL-7 showed transcriptional profiles similar to those of *ex vivo*-derived cells (Fig. S5a to d), with 70% to 90% of pathways not showing differences in expression between *ex vivo* and *in vitro*

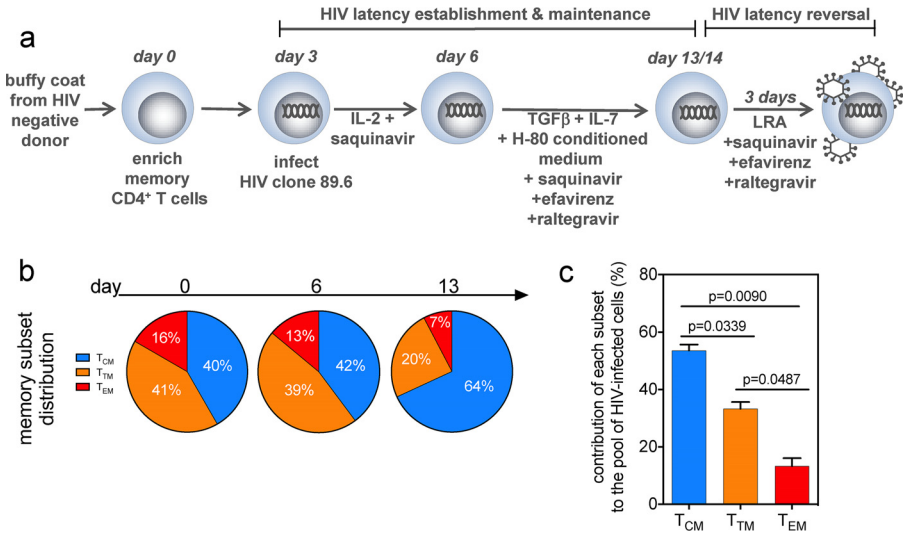

FIG 5 *In vitro* model of HIV latency LARA recapitulates the dynamics of HIV infection in memory CD4$^+$ T cell subsets. (a) Schematic of the LARA model. On day 0, resting memory CD4$^+$ T cells are enriched and allowed to rest before infection on day 3 with the full-length replication-competent HIV clone 89.6. Immediately after spinoculation, cells are resuspended in IL-2 and saquinavir. Infected cells are incubated for an additional 3 days before being introduced into latency culture conditions on day 6. Latency culture medium contains TGF-β, IL-7, conditioned medium from the H-80 cell line, and an antiretroviral cocktail of saquinavir, efavirenz, and raltegravir. After 7 days, the latently infected cells are exposed to LRAs in the presence of the triple-antiretroviral cocktail. Latency reversal is quantified by assessing percentages of CD4$^-$ Gag$^+$ cells by flow cytometry. (b) The memory cell subset distribution was monitored on days 0, 6, and 13 in LARA culture. The proportions of the population in the T_{CM}, T_{TM}, and T_{EM} subsets at each time point are indicated in the pie slices ($n = 23$). (c) The contribution of each subset to the pool of HIV-infected cells was determined. On day 13, latently infected cells generated in the LARA were sorted into T_{CM}, T_{TM}, and T_{EM} populations and were assessed for the presence of integrated HIV DNA by quantitative PCR. The contribution of each subset is expressed as the frequency of integrated HIV DNA by the proportion of cells present in each subset in the total population. Paired *t* test *P* values are indicated (error bars indicate SD; $n = 3$).

cells. Changes in gene signatures were observed mostly in pathways downstream of TGF-β signaling, i.e., the downregulation of inflammatory pathways (IFN-γ, inflammatory response, TNF-α signaling) and metabolic pathways (oxidative phosphorylation, targets of MYC, mTORC1, a pathway critical for effector memory T cell differentiation) (Fig. 6a; Table S6) (75, 76). Importantly, T_{EM} cells exposed to TGF-β still expressed higher levels of the transcriptional machinery involved in effector T cell function and HIV transcription and replication (EOMES, CCL5, IL-18RAP, STAT5, NFATC2) than T_{CM} cells (Fig. 6b and c). These results confirm that LARA culture conditions uniquely retain phenotypically and transcriptionally distinct memory CD4$^+$ T cell subsets that allowed us in a single assay to assess LRA activity in each memory subset and differential examination of the dynamics of HIV latency reversal.

The LARA shows that T_{CM}, T_{TM}, and T_{EM} subsets display different efficiencies in their response to latency reversal agents. We next quantified the frequency of cells that show latency reversal in each memory CD4$^+$ T cell subset. Anti-CD3 and CD28 antibody TCR engagement was used to reactivate HIV from latently infected cells generated in the LARA and subsequently was the positive control for all LARA HIV reactivation (77–80). Activation with anti-CD3 and CD28 antibodies for 72 h resulted in a median 12-fold increase in the frequency of CD4$^-$ Gag$^+$ cells in the total memory CD4$^+$ population ($P < 0.0001$) (Fig. 7a). Our results also show increased frequencies of CD4$^-$ Gag$^+$ cells upon TCR stimulation in all memory CD4$^+$ T cell subsets, with T_{CM} cells showing the highest fold increase compared to the frequencies in T_{TM} cells ($P = 0.0005$) and T_{EM} cells ($P = 0.07$), with a median increase of 14-fold in T_{CM}, 4-fold in T_{TM}, and 9-fold in T_{EM} cells (Fig. 7b). To demonstrate the impact of TGF-β and IL-7 on HIV latency in the LARA, we omitted each cytokine alone or in combination and examined the resulting frequency of CD4$^-$ Gag$^+$ cells after activation with anti-CD3

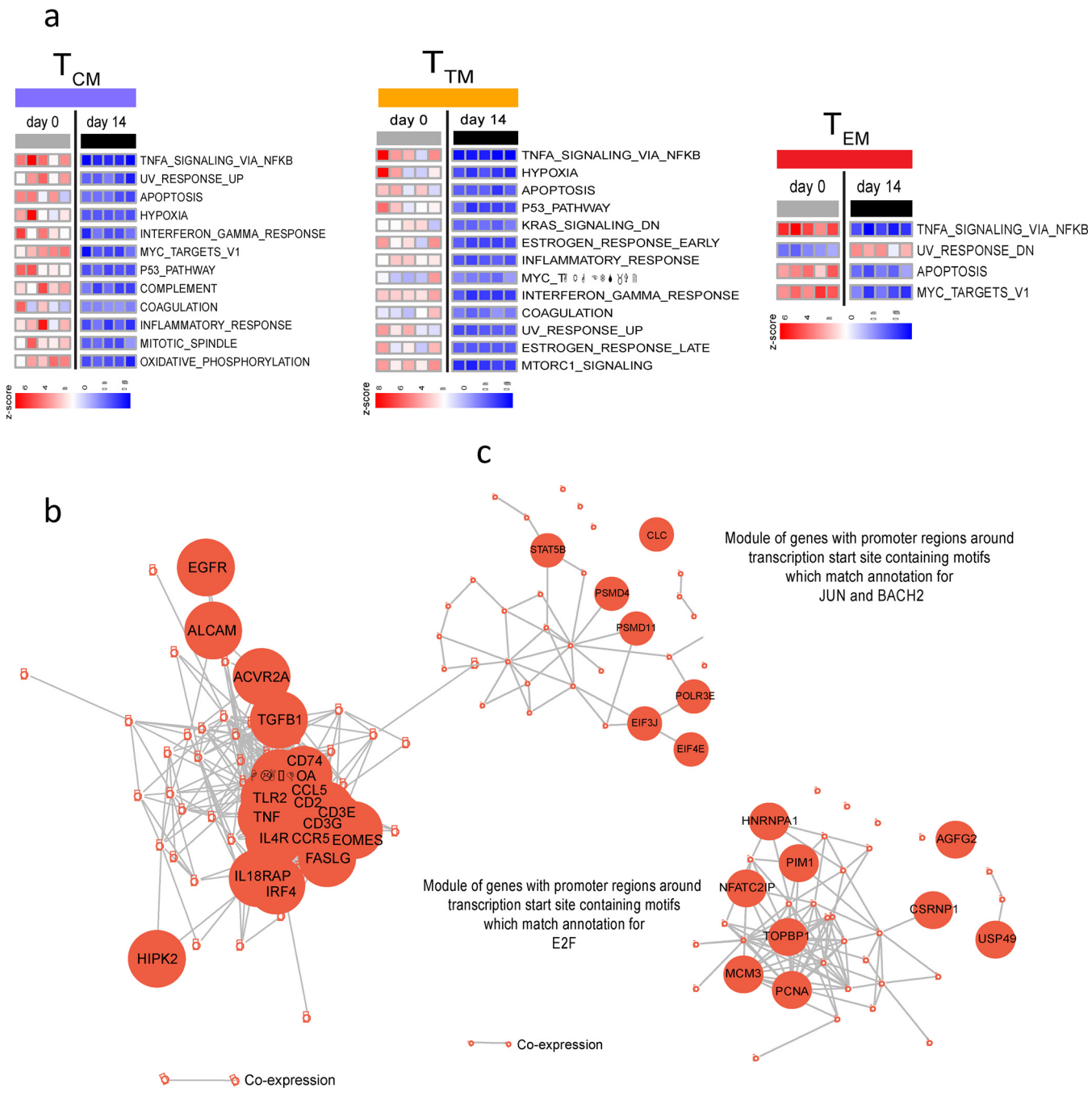

FIG 6 Transcriptional profiling of memory subsets from LARA cultures. (a) Pathways significantly (P value $<$ 5%) enriched among the genes differentially expressed in a comparison of day 14 to day 0 results for T_{CM}, T_{TM}, and T_{EM} cells, respectively, by GSEA. The expression of pathways in each sample is represented by their z-scores, calculated using SLEA. The rows represent pathways, and columns represent samples. (b) GSEA of the genes differentially expressed between the T_{EM} and T_{CM} subsets in the LARA *in vitro* (day 14) culture using the Hallmark gene sets of MSigDB. Represented are the network of genes of the Hallmark allograft rejection pathway and the IL-2 STAT5 signaling pathway upregulated in effector memory cells (T_{EM}) (P values $<$ 5%), with edges inferred by GeneMANIA showing coexpression between genes, with certain genes of the pathways highlighted in larger nodes. (c) GSEA of the genes differentially expressed between T_{EM} and T_{CM} subsets in LARA *in vitro* culture, using the gene sets that share transcription factor binding sites defined in the C3 gene sets (TRANSFAC version 7.4) of MSigDB. The gene sets upregulated in T_{EM} cells at a P value of $<$0.05 were grouped into related modules by the enrichment map strategy. Modules were defined if gene sets had an overlap of at least 25% genes between them. The genes represented in at least 50% of gene sets of a module and the edges inferred by GeneMANIA as being coexpression between genes are represented.

and CD28 antibodies ($n = 3$) (Fig. S4c). Activation under standard LARA conditions resulted in the induction of ~16.6% of $CD4^-$ Gag^+ cells, an average 8.5-fold increase over the percentage in the unstimulated control (Fig. S4c). Omission of both cytokines results in a very low frequency of $CD4^-$ Gag^+ cells (~1.8%; 1.5-fold increase), while

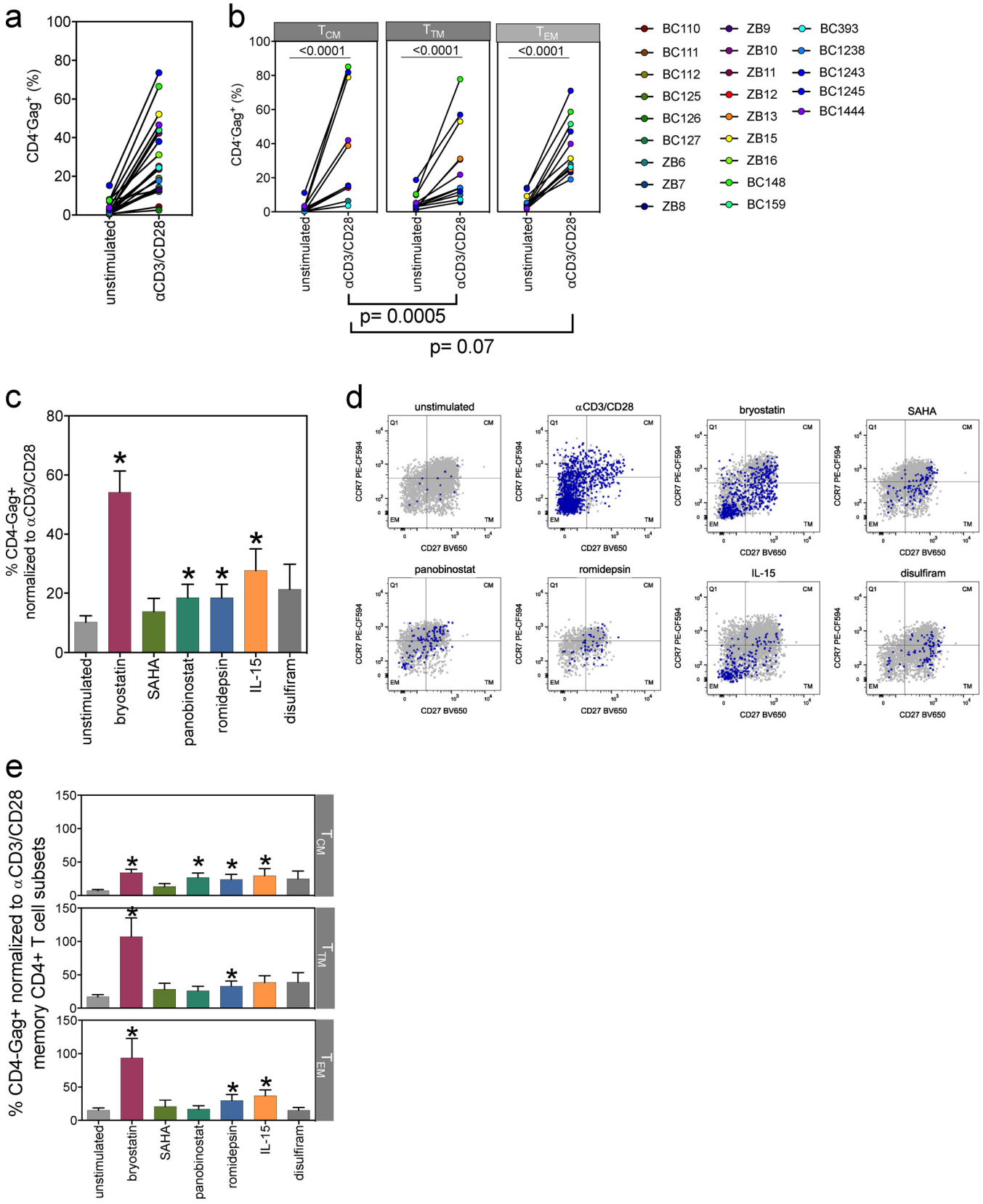

FIG 7 LRAs induce differential responses in different memory CD4$^+$ T cell subsets. (a) Anti-CD3 (αCD3) CD28-activated cells generated in the LARA show a significant increase in the CD4$^-$ Gag$^+$ population over the background level (each circle represents a unique donor in individual assays; paired Wilcoxon rank sum test; $n = 23$, $P < 0.0001$). The mean of unstimulated cells is 3%, and the mean of anti-CD3- and CD28-activated cells is 28%. The median fold change in CD4$^-$ Gag$^+$ expression induced by anti-CD3 and CD28 antibodies is 12-fold. (b) Latency reversal was assessed in the CD4$^+$ T_{CM}, T_{TM}, and T_{EM} subsets after TCR

(Continued on next page)

omission of either TGF-β or IL-7 results in frequencies of Gag$^+$ CD4 T cells of ~6.9% (4.4-fold increase) or ~5.6% (1.4-fold increase), respectively.

We next quantified the response of latently infected memory CD4$^+$ T cells in the LARA to *ex vivo* CD4$^+$ T cells from virally suppressed HIV-infected individuals from the FL cohort using TILDA and several classes of LRAs, including bryostatin, the HDAC inhibitors (HDACi) panobinostat, romidepsin, and suberoylanilide hydroxamic acid (SAHA), the acetaldehyde dehydrogenase inhibitor disulfiram, and IL-15. We determined the frequency of infected cells in each assay and then assessed the maximal responsiveness of each participant to anti-CD3 and CD28 antibody stimulation in the LARA ($P = 0.0187$; $n = 5$) (Fig. S6a) or PMA plus ionomycin stimulation in *ex vivo* CD4$^+$ T cells using TILDA ($P = 0.0284$, $n = 4$) (Fig. S6b) (27). Bryostatin (50 nM), panobinostat (20 nM), romidepsin (20 nM), and IL-15 (10 ng/ml) significantly induced latency reversal in memory CD4$^+$ T cells in the LARA (P value < 0.05), with bryostatin showing the highest efficiency (mean, 25%) (Fig. S6c). The HDACi SAHA (0.5 μM) showed the lowest latency reversal (mean, 11%). Bryostatin showed the highest efficiency in latency reversal (Fig. S6d) (mean, 20%; $P = 0.0419$) in *ex vivo* CD4$^+$ T cells from virally suppressed HIV-infected individuals. All other LRAs showed lower efficiency in reactivating HIV, including HDACi, in *ex vivo* samples (<10% of positive control), most probably a result of the lower frequency of cells with integrated provirus in these samples than in LARA samples. These data show that the LARA identified classes of LRAs with a hierarchy of latency reversal effectiveness that recapitulated TILDA results obtained with *ex vivo*-sorted subsets (Fig. 2b). These results validated the use of the LARA as a platform to predict the efficacy of LRAs to reactivate HIV in each memory subset.

To further characterize the response to LRAs, we identified the 50% effective concentration (EC_{50}) for each compound (data not shown) and assessed the responsiveness to LRAs of the total memory population as well as each memory CD4$^+$ T cell subset in the LARA. Memory CD4$^+$ T cells showed a range of responses to bryostatin, SAHA, panobinostat, romidepsin, IL-15, and disulfiram that resulted from the differential responses of each memory subset (Fig. 7c to e). Although latency reversal with bryostatin was significant in all subsets (P value < 0.05), it showed the highest efficiency in T_{TM} (mean, >100%) followed by T_{EM} (mean, 94%) and T_{CM} (mean, 34%) cells. Romidepsin also demonstrated significant latency reversal (P value < 0.05), but the overall efficiency for any subset was low (mean, ≤33%). The latency reversal efficiency of IL-15 was significant (P value < 0.05) in T_{CM} (mean, 29%) and T_{EM} (mean, 37%) cells. We showed that LRAs can induce *ex vivo* CD4$^+$ T cell activation and differentiation, i.e., PMA plus ionomycin and bryostatin (Fig. 2). To determine if LRA-induced latency reversal could be attributed to the differentiation of T_{CM} cells into more differentiated subsets (81, 82), we quantified T_{CM}, T_{TM}, and T_{EM} cell frequencies prior to and upon exposure to LRAs (Fig. 8a). T_{TM} cell frequencies significantly decreased upon exposure to all LRAs except disulfiram, while T_{EM} cells significantly increased after exposure to all tested compounds (P value < 0.05) (Fig. 8a). Anti-CD3 and CD28

FIG 7 Legend (Continued)
stimulation with anti-CD3 and CD28 antibodies (paired Wilcoxon rank sum test, $P < 0.001$ for each memory subset). The mean of the CD4$^-$ Gag$^+$ cell population in the T_{CM} subset negative control was 2%, the mean of the TCR-activated cell population was 33%, and the median was a 14-fold change. The mean of the CD4$^-$ Gag$^+$ cell population in the T_{TM} subset negative control was 6%, the mean of the TCR-activated cell population was 28%, and the median was a 4-fold change. The mean of the CD4$^-$ Gag$^+$ cell population in the T_{EM} negative control was 6%, the mean of the TCR-activated cell population was 37%, and the median was a 9-fold change ($n = 12$). We examined different classes of LRAs for efficiency of latency reversal in the LARA. (c) Percentages of CD4$^-$ Gag$^+$ cells within total memory CD4$^+$ T cells after exposure to each compound were normalized to the percentage of the positive control with 1 μg/ml anti-CD3 and CD28 antibodies. LRA concentrations shown are 5 nM bryostatin (maroon bar), 1 μM SAHA (olive bar), 20 nM panobinostat (green bar), 5 nM romidepsin (blue bar), 500 ng/ml IL-15 (orange bar), and 1 μM disulfiram (dark-gray bar). $n = 10$. (Error bars indicate standard errors of the means [SEM]; asterisks indicate a P value of <0.05 in a comparison of the drug with the unstimulated controls, tested by a paired Wilcoxon rank sum test.) LRAs trigger different quantitative responses in memory CD4$^+$ T cell subsets. (d) Representative flow plots show responses from one LARA donor. The *x* and *y* axes represent CD27 and CCR7 expression in the CD45RA$^-$ memory compartment, respectively. Gray dots represent the entire memory population present in the sample overlaid with CD4$^-$ Gag$^+$-expressing cells (purple) to show localization within the memory subsets. Each subset is identified within the flow cytometry plot. (e) Latency reversal efficiency from LARA donors in panel c was assessed in the T_{CM} (top), T_{TM} (middle), and T_{EM} (bottom) subsets. The percentage of CD4$^-$ Gag$^+$ cells expressed in each subset was normalized to the signal from the positive control with anti-CD3 and CD28 antibodies ($n = 10$; error bars indicate SEM; asterisks indicate a P value of <0.05 for a comparison of the drug with unstimulated controls, tested by a paired Wilcoxon rank sum test).

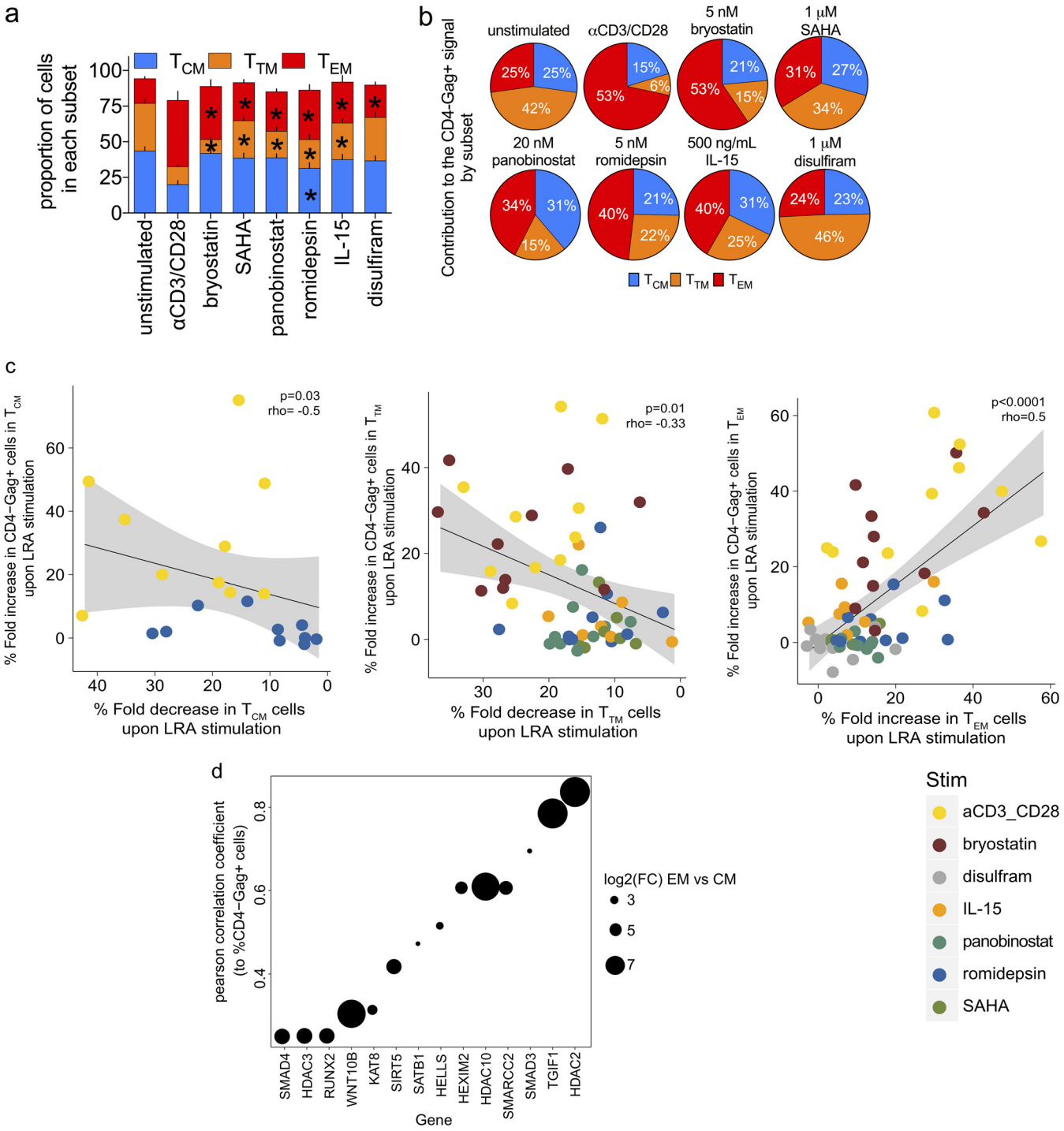

FIG 8 The T_{EM} subset shows the greatest contribution to latency reversal from different classes of LRAs. (a) The effect of LRAs on the distribution of the memory $CD4^+$ T cell subsets was assessed and is represented by the percentage of cells in each subset in the $CD45RA^-$ population (bars indicate SEM; asterisks indicate a *P* value of <0.05 in a comparison of the drug with unstimulated controls in each memory subset, tested by a paired Wilcoxon rank sum test). (b) The contribution of the T_{CM}, T_{TM}, and T_{EM} subsets to the overall $CD4^-$ Gag^+ signal for each LRA was determined. Each pie slice was calculated using the frequency of cells in each memory subset from the $CD4^-$ Gag^+ population. Frequency is indicated within each pie slice. $n = 10$. (c) Correlation between the percent change in $CD4^-$ Gag^+ cells after LRA stimulation and the percent change in cells in the T_{EM}, T_{TM}, and T_{CM} subsets after exposure to LRAs. Each circle represents an independent donor after administration of anti-CD3 CD28 (yellow), bryostatin (brown), disulfiram (gray), IL-15 (orange), panobinostat (green), romidepsin (blue), or SAHA (olive). *P* values of Spearman's correlation test are indicated. (d) Genes of the HDAC gene sets expressed at day 14 in LARA *in vitro* culture in T_{CM} and T_{EM} cells correlated with the percentage of $CD4^-$ Gag^+ cells measured postreactivation in T_{CM} and T_{EM} cells by anti-CD3 and CD28 antibody stimulation. The enrichment of gene sets was tested by GSEA using the PID HDAC pathway gene sets and custom gene sets as the database (enrichment *P* value < 0.05). The genes are represented on the *x* axis, and the Pearson correlation coefficient of each gene to the HIV msRNA is represented on the *y* axis. The size of the dots represents the $\log_2$ fold change of the gene in T_{EM} cells compared to that in T_{CM} cells.

antibodies and romidepsin were the only conditions to significantly decrease frequencies of T_{CM} cells (P value < 0.05). These data suggest that after exposure to LRAs, T_{TM} cells may transition more readily to T_{EM} cells. The relative contributions of the memory $CD4^+$ T cell subsets to the total $CD4^-$ Gag^+ signal were varied (Fig. 8b). Similarly to what we observed in *ex vivo* T_{EM} cells (mean, 52%) (Fig. 1d), T_{EM} cells in the LARA contributed the most to frequencies of $CD4^-$ Gag^+ cells after anti-CD3 and CD28 antibody stimulation (mean, 53%) (Fig. 8b). Indeed, T_{EM} cells, which comprised the smallest proportion of the $CD4^+$ T cell population (Fig. 5b) (mean, 7%), contributed the most to the $CD4^-$ Gag^+ signal for all but two of the compounds tested, SAHA and disulfiram (Fig. 8b). In contrast, T_{CM} cells, which comprised 60% of the total population and greater than half the HIV-infected cell population (Fig. 5b), comprised only 21 to 31% of the frequency of $CD4^-$ Gag^+ cells induced from all compounds tested (Fig. 8b). These data confirm the differential responses of memory $CD4^+$ T cell subsets to LRAs. Further, they show that the contribution to latency reversal in $CD4^+$ T cell subsets is derived predominantly from the T_{EM} subset phenotype.

Due to the observed changes in the subset distribution after LRA exposure, we next determined whether the magnitude of these changes induced by all LRAs correlated with latency reversal in our model. We had observed that TCR stimulation, bryostatin, disulfiram, IL-15, panobinostat, romidepsin, and SAHA all led to significantly increased frequencies of T_{EM} cells after 72 h of culture (Fig. 8a). Comparison of the fold increase in numbers of T_{EM} cells after LRA exposure revealed a significant correlation with increased induction of HIV Gag expression (Fig. 8c) ($P < 0.0001$). As expected, a significant decrease in the T_{CM} and T_{TM} cell frequencies also correlated with increased HIV Gag^+ cells upon LRA exposure (T_{CM} cell $P = 0.03$; T_{TM} cell $P = 0.01$) (Fig. 8c). Together, our data indicate that LRAs which can induce quiescent T_{CM} cells to progress into more differentiated T_{EM} cells will trigger the highest latency reversal efficiency.

T_{EM} cells show the epigenetic machinery that is required to trigger HIV p24 in the LARA. In Fig. 4, we showed that the expression of several members of the HDAC gene family were expressed at higher levels in *ex vivo*-isolated T_{EM} cells than in T_{CM} cells and that this upregulated expression of activators and inhibitors of epigenetic changes was correlated with increased frequencies of inducible HIV msRNA. We used transcriptional profiling to test for the enrichment (using gene set enrichment analysis [GSEA]) of the HDAC gene set in T_{EM} cells and T_{CM} cells on day 14 of the LARA and quantified their correlation with the frequency of $CD4^-$ Gag^+ cells postreactivation in the memory subsets (Fig. 8d). Increases in HDAC gene expression (e.g., HDAC2, HDAC3, HDAC10), SATB1 (known to recruit HDACs), epigenetic silencers (RUNXs), and SMARCAs (which includes a helicase that controls cell cycle entry, HELLS [83]) in addition to HATs (like KAT8) on day 14 of culture correlated with an increase in the frequency of $CD4^-$ Gag^+ cells postreactivation (normalized enrichment score > 1.5; enrichment P value < 0.05). Moreover, all these genes showed higher expression in T_{EM} cells than in T_{CM} cells ($\log_2$ fold change, T_{EM} cells versus T_{CM} cells, 3 to 7) (Fig. 8d). These results confirm that T_{EM} cells are poised to express HIV upon stimulation with LRAs as they preferentially express genes known to control latency and reactivation.

DISCUSSION

We characterized the impact of mature T cell differentiation as defined by the memory $CD4^+$ T cell subset transcriptional profile and phenotype on latency reversal using both *ex vivo* $CD4^+$ T cells from virally suppressed participants and a newly developed *in vitro* model of HIV latency, the LARA. Latency reactivation is thought to occur in activated cells and/or in cells undergoing active cycling and apoptosis (84–87). Our data demonstrated, *ex vivo* and *in vitro*, that T_{EM} cells had the largest inducible HIV reservoir and the highest contribution to the latency reversal signal. Our results also showed that LRAs can trigger quiescent T_{CM} cells and T_{TM} cells to differentiate and acquire cell surface phenotypes, effector functions, and signal transduction pathways which characterize T_{EM} cells. Notably, these changes in transcriptional profiles also involved the upregulation of genes that promote HIV reactivation and replication, and

these changes correlated with the induction of HIV expression. Together, these data support differentiation into an effector memory phenotype to be an effective pathway to latency reversal.

We demonstrated that T_{CM} cells, T_{TM} cells, and T_{EM} cells showed distinct responses to LRAs, which is associated with changes in biological pathways specific to each subset. In the T_{CM} cell subset, bryostatin induced downregulation of FOXO1 targets. Loss of FOXO1 expression and of its downstream transcriptional targets triggers the differentiation of T_{CM} cells to effector cells and an activated effector phenotype (88). Our results also show that T_{EM} cells express several genes that control the induction of HIV latency (HDACs, SMARCAs), as well genes which can enhance reactivation and replication of HIV. Transcriptional profiling revealed that T_{EM} cells expressed pathways that support HIV production, including the PKC activation pathway, AP-1 and E2F transcription factor target and proinflammatory pathways, and the NF-κB and nuclear factor of activated T cell (NFAT) pathways, all of which were associated with greater LRA responsiveness. Multivariate modeling of phenotypic analysis of *ex vivo* cells showed proliferation and cell surface markers of T cell activation to be the best predictors of inducible HIV msRNA reactivation. They also showed that the differentiation of T_{CM} cells and T_{TM} cells triggered by LRAs to cells that express the T_{EM} cell phenotype and transcriptional profile was associated with the magnitude of latency reversal.

We also identified that changes in pathways of chromatin remodeling are associated with the inducible HIV reservoir predominantly in the T_{EM} subset after LRA treatment in *ex vivo* $CD4^+$ T cells from virally suppressed participants and that expression of these pathways predicts the efficiency of latency reversal in our *in vitro* model. The T_{EM} subset is characterized by rapid response to antigen by the upregulation of effector genes. Epigenetic modulation is a mechanism of regulating gene expression, which is controlled by chromatin remodeling pathways, such as HDACs and SMARCAs. The low expression of these pathways in highly quiescent subsets, such as T_{CM} cells, show the downregulated expression of these regulatory genes. Other studies have previously demonstrated the T_{EM} subset to have more open chromatin than the T_{CM} subset, correlating with fast kinetics of effector function responses upon activation (20). Here, we show that the gene signatures of higher HDAC expression correlate with a highly inducible reservoir, suggesting a differential mechanism of HIV latency control. HDAC inhibitors like SAHA (vorinostat) have been examined in clinical trials for HIV eradication (89, 90) but have had limited demonstrable success in facilitating reservoir clearance. Our results here confirm that approaches that modulate epigenetic pathways not limited to HDACs are a significant component of HIV latency reversal. Enhancing the induction of critical transcription factor targets in each memory $CD4^+$ T cell subset in combination with epigenetic pathway changes may provide a pathway to enhance latency reversal *in vivo*. Differentiation of long-lived T_{CM} cells by LRAs into T_{EM} cells, known to have a more limited life span and higher turnover rate, may provide a novel strategy that results in the accelerated decay of the HIV reservoir.

T_{EM} cells have been shown to harbor more intact proviruses than T_{CM} cells (24), while also maintaining a higher proliferation rate and a shorter half-life (91, 92) than those of T_{CM} cells (intermitotic times, 15 days and 48 days, respectively [14]). Using TILDA on sorted memory $CD4^+$ subsets, we show the capacity of the epigenetic and transcriptional status of each subset to support the LTR-driven expression of multispliced HIV RNA and that T_{EM} cells harbor the highest frequency of cells induced to express HIV RNA even after normalization to the frequency of copies of integrated provirus. These data provide evidence that T_{EM} cells provide an ideal cellular environment to support HIV replication upon activation. LASSO regression analysis identified *ex vivo* markers of each subset that correlated with the highest frequency of the measured inducible HIV reservoir after stimulation, including Ki67 in T_{CM} cells and PD-1, CD127, and Ki67 in T_{EM} cells, suggesting that the subsets expressing these markers were important in defining the frequencies of latently infected cells.

The mechanism for how T_{EM} cells maintain a higher frequency of intact provirus is not well understood, and future studies will focus on characterizing the role of the T cell

phenotype in infection, establishment of latency, and HIV persistence. Interestingly, multiple studies have demonstrated T_{EM} cells to be very sensitive to cytotoxic T lymphocyte (CTL)-mediated killing (93, 94). However, elimination of cells infected with replication-competent HIV is hampered by the expression of viral proteins that mediate evasion of immune system detection (nef, env) (95–98) or induce cell cycle arrest (vpr) (99, 100), which may limit the effective clearance of infected T_{EM} cells *in vivo*.

We also present a model of HIV latency, the LARA, that allowed us to examine latency establishment, maintenance, and reversal in memory $CD4^+$ T cell subsets. In this model, TGF-β, a pleiotropic mediator of broad aspects of cell development and homeostasis (101, 102) with well-characterized potent inhibitory effects on $CD4^+$ T cell proliferation and differentiation (29, 66–69), was employed to induce HIV latency. A study by Barouch et al. showed in a simian immunodeficiency virus (SIV) model that triggering of the TGF-β signaling pathway in all lymphoid tissues was one of the earliest events after HIV infection that correlated strongly with viral dissemination and was concomitant with suppression of innate immunity and likely seeding of the reservoir (103). TGF-β is produced by T cell regulators (Tregs), a subset of cells known to be present in lymph nodes, a major site of HIV persistence (104). Hence, the use of TGF-β in the LARA to establish and maintain HIV latency exploits a pathway that triggers T cell quiescence *in vivo*. We provide a rationale extending the role of this pathway in the establishment and reversion of HIV latency which should lead to the development of strategies that target TGF-β to reactivate HIV from latent stores. In addition to TGF-β signaling, γ-chain family cytokine IL-7 signaling has been shown to be essential for T cell survival and homeostasis (46, 105–107) and to promote HIV persistence *in vitro* and *in vivo* (70, 71, 108, 109). The antagonistic effect of TGF-β allowed the addition of IL-7 in the LARA for the maintenance of memory $CD4^+$ T cells subsets without triggering increased viral replication (110). Analysis of transcriptional profiles confirmed that memory $CD4^+$ T cell subsets in the LARA maintained their phenotype after 14 days of *in vitro* culture and showed that the perturbed pathways were mostly those downstream of TGF-β. Coincidentally, T_{CM} cells show the highest enrichment in TGF-β-regulated genes and include mostly genes that inhibit cell cycle entry and T cell activation; expression of these genes by T_{CM} cells may provide a mechanism that explains their refractoriness to HIV reactivation. Together, these conditions support TGF-β as an extrinsic signal that can trigger the establishment and maintenance of latent HIV-infected T_{CM}, T_{TM}, and T_{EM} cells in the LARA.

Using the LARA model, we show that the increase in the number of cells with an effector memory phenotype after treatment with any LRA, including anti-CD3 CD28 cells, is significantly correlated with latency reversal. The proportion of cells transitioning within the $CD4^+$ T cell population from the T_{CM} to the T_{EM} phenotype correlates with increased latency reversal. Importantly, although we do observe changes in cell surface markers specific to T_{CM} upon addition of an LRA, transcriptional profiling of these cells highlights the increased expression in these T_{CM} cells of genes that are involved in the acquisition of effector function and that support HIV replication. Significantly, previous studies have demonstrated that responses to anti-CD3 CD28 costimulation specifically result in an increase in effector function in these cells (111, 112), supporting a role for transition from quiescence to effector function in latency reversal. We also note that our *in vitro* latency model employs the protease inhibitor saquinavir immediately after memory $CD4^+$ T cells are exposed to the replication-competent virus; this limits the infection to a single round and also limits the accumulation of inactivating mutations or deletions that may be observed in the *ex vivo* samples, which can influence the observed frequency of HIV latency reversal. Additionally, our positive control for the LARA system is anti-CD3 CD28 activation. T_{CM} cells express high levels of CD28 and therefore may be more responsive specifically to this mechanism of activation, which may provide a higher activation signal to the T_{CM} subset than to the other subsets.

Here, we have confirmed in two experimental systems, i.e., *ex vivo* analysis of T cell subsets and analysis of reactivation of HIV in an *in vitro* model of latency, that

expression by T_{EM} cells of genes involved in T cell activation/proliferation supports a cellular environment which is more favorable to HIV replication and which can explain their enhanced response to LRAs compared to those of T_{CM} or T_{TM} cells. These data suggest that efficient LRAs need to trigger a transcriptional program that will lead to the differentiation of highly quiescent cells with an activated phenotype capable of supporting HIV replication, i.e., T_{CM} to T_{EM} cells. IL-15, a cytokine known to trigger the differentiation of T_{CM} into T_{EM} cells also was shown to induce HIV expression from latently infected cells. Our results also suggest that anti-inflammatory cytokines, including TGF-β, may be potential targets for antibodies that can neutralize their capacity to inhibit innate and adaptive immune responses and to induce HIV latency. Our data suggest that Tregs, which produce TGF-β, may also be targeted to facilitate reactivation of latent HIV. Recent reports have shown that depletion of Tregs in SIV-infected aviremic nonhuman primates restores SIV replication (104). Strategies that target anti-inflammatory cytokines, such as TGF-β, also promote memory T cell differentiation, which as our results suggest results in HIV production. Overall, our findings pave the way for novel interventions that can restore HIV production and make the virus visible to a rejuvenated immune system capable of eliminating virally infected cells.

MATERIALS AND METHODS

Participants and samples. Forty-seven HIV-infected participants receiving suppressive ART were recruited at the University of California, San Francisco (UCSF). Participants received ART for >3 years and had a $CD4^+$ T cell count of >350 cells/μl and an HIV RNA level of <40 copies/ml, as measured by the Abbott real-time HIV-1 PCR for at least 3 years. Whole blood (50 ml) was collected by regular blood drawing. All participants signed informed consent approved by the UCSF review board.

Twenty-two additional HIV-infected participants were recruited at the Midway Immunology Research Center (Fort Pierce, FL). All participants signed informed consent approved by the Martin Memorial Health Systems review board. None of the participants under ART experienced any detectable plasma viremia at the time of study, as assessed by viral load measurement using the AmpliPrep/Cobas TaqMan HIV-1 test (v 2.0; Roche), with a detection limit of 20 copies/ml of plasma. All four individuals had been on successful ART for >36 months. All participants underwent leukapheresis to collect large numbers of PBMCs.

Cell culture. Primary memory $CD4^+$ T cells and H-80 cells were maintained in RPMI 1640 medium (Cellgro; 10-040-CV) supplemented with 10% fetal bovine serum (FBS; PAA; A15-752), 1% penicillin-streptomycin (Cellgro; 30-001-CI), and 1% HEPES (Gibco; 15630-080) complete cRPMI (cRPMI). H-80 feeder cells (U-251 MG; Cell Lines Service) were maintained as a monolayer to a maximum 80% confluence. 293 cells used for virus production were maintained as a monolayer in Dulbecco's modified Eagle's medium (DMEM; Gibco; 11995-065) plus 10% fetal bovine serum and 1% penicillin-streptomycin (cDMEM).

Plasmid preparation. The following reagent was obtained through the NIH AIDS Reagent Program, Division of AIDS, NIAID, NIH: p89.6 from Ronald G. Collman (113–115). p89.6 that had been transformed into *Escherichia coli* was grown overnight in the presence of ampicillin at 30°C, and plasmid preparations were subsequently made using a Qiagen maxiprep kit (Qiagen; 12963) according to the manufacturer's protocol. Plasmid DNA was resuspended in elution buffer to a final concentration of 1 μg/μl.

Virus production. Ninety times 10^6 low-passage-number 293 cells were seeded into 10-layer CellBIND Surface HYPERFlask M cell culture vessels (Corning; 10030) in cDMEM and allowed to adhere overnight at 37°C in 5% CO_2. The next day, 293 cells were transfected with p89.6 DNA by using 25-kDa linear polyethylenimine (PEI; Polysciences, Inc.; 23966) as a carrier and 150 mM NaCl as a diluent. Cells were incubated with the transfection cocktail in the HYPERFlask for 1 day before the medium was exchanged for UltraCULTURE serum-free medium without L-Gln (Lonza; 12-725F) containing 1% HEPES, 1% GlutaMAX (Gibco; 35050-061), and 0.6 mg/ml glucose. The transfected 293 cells were then incubated for an additional 2 days. Viral supernatants were then collected, filtered (Sigma; Z358274-12EA filter), and treated with DNase I (Invitrogen; 18068-015) for 30 min at 37°C to remove any residual plasmid DNA before being aliquoted and stored at −80°C.

Isolation of total $CD4^+$ T cells. PBMCs were isolated from leukapheresis products by Ficoll-Hypaque density gradient centrifugation and cryopreserved in liquid nitrogen. After PBMC thawing, total $CD4^+$ T cells were isolated from cryopreserved PBMCs by negative selection according to the manufacturer's protocol with the EasySep human $CD4^+$ T cell enrichment kit (Stemcell Technologies; 19052).

Isolation, spinoculation, and culture of $CD4^+$ T memory lymphocytes. For LARA culture, PBMCs were isolated by Ficoll-Hypaque density gradient centrifugation of buffy coats from HIV-negative healthy donors. PBMCs were immediately processed to enrich for memory $CD4^+$ T cells by negative selection according to the manufacturer's protocol with the EasySep human CD4 memory T cell enrichment kit (Stemcell Technologies; 10157). Purified memory $CD4^+$ T cells (>98%) were allowed to rest in cRPMI at 37°C in 5% CO_2 for 3 days at a density of 2×10^6 cells/ml. Following the resting period, cells were spinoculated at 2,500 rpm for approximately 2.5 h at 30°C with 89.6, a replication-competent clinical isolate (113–115), at 100 ng/ml p24/million $CD4^+$ T cells. Polybrene (Sigma; H9268) was added to a 1-μg/ml final concentration. Cells were spinoculated at 2,500 rpm for approximately 2.5 h at 30°C. After

spinoculation, the viral supernatant was removed and infected cells were cultured at a density of 1×10^6 cells/ml in cRPMI supplemented with 30 U/ml IL-2 (R&D Systems; 202-IL) and 5 μM saquinavir (NIH AIDS Reagent Program; 4658) at 37°C in 5% CO_2 for 3 days. The antiretroviral drugs were added to suppress viral spread and to prevent preintegration latency. On day 6, purified $CD4^+$ T memory cells were resuspended at 2×10^6 cells/ml in a latency cocktail of 50% cRPMI, 50% supernatant harvested from an H-80 feeder cell line, 20 ng/ml recombinant human TGF-β1 (PeproTech; 100-21C), 40 ng/ml recombinant human IL-7 (R&D Systems; 207-IL), and an antiretroviral cocktail of 100 nM efavirenz, 200 nM raltegravir, and 5 μM saquinavir (NIH AIDS Reagent Program; 4624, 11680, and 4658). On day 10, half of the culture medium was replaced with freshly prepared latency cocktail and culture volume was adjusted to maintain the cellular density of 2×10^6 cells/ml. Cells were harvested on day 13 or 14. For phenotypic and virologic analyses, cell samples were taken on days 0, 3, 6, 8, 10, and 14.

Latency reversal with LRAs in the LARA. On day 13 of the LARA, cells were washed, counted, and plated for latency reversal at a density of 1×10^6 cells/ml in cRPMI in the presence of 100 nM efavirenz, 200 nM raltegravir, and 5 μM saquinavir and the LRA indicated. Cells were stimulated with1 μg/ml plate-bound OKT3 and 1 μg/ml soluble CD28 (BioLegend; 302933), bryostatin (Aphios; APH-09061), SAHA (a generous gift from Merck & Co., Inc., Kenilworth, NJ, USA), panobinostat (Selleckchem; LBH589), romidepsin (APExBIO; FK228), disulfiram (APExBIO; A4015), or IL-15 (R&D Systems; 247-ILB). Cells were harvested after 72 h and analyzed by flow cytometry.

Antibody labeling of cells for flow cytometry. Cells were incubated for 30 min at 4°C with fluorescence-labeled antibodies to surface markers in phosphate-buffered saline (PBS) plus 4% FBS. After being washed, cells were fixed in PBS plus 2% paraformaldehyde for 30 min at 4°C and then used for flow cytometry analysis. For intracellular Gag detection after surface antibody staining, cells were fixed in PBS plus 2% paraformaldehyde for 10 min at room temperature before permeabilization with 0.25% saponin. Cells were then incubated with Gag fluorophore-conjugated antibody (Beckman; 6604667) in the presence of 0.25% saponin for 30 min at room temperature. After a washing step, cells were fixed in PBS plus 2% paraformaldehyde for 30 min at 4°C. For the Treg and TH1/TH2/Tfh panels, cells were permeabilized and fixed after incubation with surface antibodies according to the manufacturer's protocol with a Foxp3/transcription factor staining buffer set (eBioscience; 00-5523-00) to detect intracellular transcription factors. After a washing step, cells were fixed in PBS plus 2% paraformaldehyde for 30 min at 4°C. Cells from all panels were washed and resuspended in PBS plus 4% FBS prior to flow cytometric analysis.

Antibody panels used in these studies were as follows: the memory $CD4^+$ T cell subset panel CD8 Pacific Blue (BD; 558207), ViViD Live/Dead aqua (Invitrogen; L34957), CD4 allophycocyanin (APC) (BD; 555349), CD27 BV650 (BioLegend; 302827), CD3 A700 (BioLegend; 300323), CD45RA APC-H7 (BD; 560674), and CCR7 phycoerythrin (PE)-Cy7 (BD; 557648). The memory subset sorting panel was as follows: CD3 fluorescein isothiocyanate (FITC) (BD; 555339), CD8 Pacific Blue (BD; 558207), CD4 APC (BD; 555349), CD45RA APC-H7 (BD; 560674), CD45RO peridinin chlorophyll protein (PerCP)-eFluor710 (eBioscience; 46-0457-42), CCR7 PE-Cy7 (BD; 557648), CD27 BV650 (BioLegend; 302827), and ViViD Live/Dead aqua (Invitrogen; L34957). For the cell cycle, we used the following: CD4 Qdot605 (Invitrogen; Q10008), CD3 PE-Cy7 (BD; 557851), CD45RA APC-H7 (BD; 560674), CD27 Qdot655 (Invitrogen; Q10066), CCR7 PE-CF594 (BD; 562381), PD-1 Alexa Fluor 647 (BD; 560838), 7-aminoactinomycin D (7-AAD) (BioLegend 420403), and Ki67 FITC (BD; 556026). For markers of activation and the proliferation panel, we used CD3 A700 (BD; 557943), CD4 Qdot605 (Invitrogen; Q10008), CD8 Pacific Blue (BD; 558207), CD45RA APC-H7 (BD; 560674), CD27 BV650 (BioLegend; 302828), CCR7 PE-Cy7 (BD; 557648), CD14 V500 (BD; 561391), CD19 V500 (BD; 561121), ViViD Live/Dead aqua (Invitrogen; L34957), HLA-DR PerCP (BD; 340690), CD38 PE (BD; 555460), CD127 PECF594 (BD; 562397), and Ki67 FITC (BD; 556026). For effector subset profiling, we used the following Treg panel: CD3 AF700 (BD; 557943), CD4 BV650 (BioLegend; 317435), ViViD Live/Dead aqua (Invitrogen; L34957), CD45RA APC-eFluor780 (eBioscience; 47-0458-42), CD25 PE-CF594 (BD; 562403), CD31 PE (BD; 560983), CD39 BV421 (BioLegend; 328213), CD127 AF647 (BioLegend; 351318), and FOXP3 AF488 (BioLegend; 320212). For the TH1/TH2/Tfh panel, we used CD3 AF700 (BD, 557943), CD4 Qdot605 (Invitrogen; Q10008), CD27 BV650 (BioLegend; 302828), CCR7 FITC (BD; 561675), CD45RA APC-H7 (BD; 560674), ViViD Live/Dead aqua (Invitrogen; L34957), CCR6 BV421 (BD; 562515), CXCR3 PE-Cy5 (BD; 561731), CXCR5 AF647 (BD; 558113), CCR4 PE-Cy7 (BD; 561034), T-bet PerCP-Cy5.5 (BioLegend; 644805), and GATA3 PE (BD; 560074).

Flow cytometry. Multicolor flow analysis of cell surface and intracellular marker expression was performed with a BD LSRII flow cytometer. Between 30,000 and 50,000 events were acquired for each sample using the live-cell gate. The data were analyzed with the FlowJo program.

Cell sorting. Central, transitional, or effector memory $CD4^+$ T cells were sorted on an Aria fluorescence-activated cell sorter (FACS) (Becton, Dickinson). Subset purity was confirmed by flow cytometry analysis on the Aria immediately postsort.

Integrated/total/2-LTR HIV-DNA. Cell samples from HIV-infected participants and from multiple time points in the LARA were used to assess the frequencies of total, integrated, and 2-LTR circle forms of HIV DNA as previously described (26).

Quantification of the inducible HIV reservoir. The size of the inducible HIV reservoir was measured through quantification of HIV msRNA expression after treatment with 100 ng/ml PMA and 1 μg/ml ionomycin or 50 nM bryostatin using TILDA as previously described (27).

Preprocessing of RNA-Seq data. Transcriptome sequencing (RNA-Seq) was performed on samples generated in the LARA from *ex vivo* (day 0) and *in vitro* culture (day 14) cells sorted on memory $CD4^+$ T_{CM}, T_{EM}, and T_{TM} subsets. RNA-Seq was also performed on memory $CD4^+$ T cell T_{CM}, T_{EM}, and T_{TM} subsets from four virally suppressed HIV-infected individuals unstimulated (negative control) or stimulated with

100 ng/ml PMA and 1 μg/ml ionomycin, 10 ng/ml IL-15, or 50 nM bryostatin for 24 h. A paired-end 50-bp run was performed on an Illumina HiSeq 2500 platform, using the TruSeq kit. An average of 9 million reads per sample was generated.

An automated pipeline developed in-house that integrates online open-source tools for processing and analyzing RNA-Seq data was used to perform processing of the sequencing data, followed by downstream analysis using R-Bioconductor packages. The sequencing raw reads were trimmed off adapter sequence contaminants using Trimmomatic (116) and mapped into the Ensembl version of the human genome (Ensembl Grch38) (117) using the STAR aligner (118). The transcript abundance was then estimated by counting the number of reads mapping to the exons that are unique to the transcripts of a gene by using HTSeq (119). The obtained transcript counts were then normalized by trimmed mean of M values (TMM) analysis, with correction for the library size (120).

Differential gene expression analysis. The differences in transcriptomic profiles between the groups to be compared were determined by fitting a generalized linear model (GLM) (121) to each transcript of the expression data, with gene expression as a dependent variable and the group as an independent variable, followed by a likelihood ratio test for the coefficients in the linear model to test whether fold changes were different from zero. These tests were conducted using the R-Bioconductor package edgeR (122). The *P* values were corrected for multiple comparisons using the Benjamin and Hochberg (BH) method (123).

Fisher's exact test was used to assess significance of overlap of genes differentially expressed between the *ex vivo* and the LARA day 14 culture memory subsets. Hierarchical clustering was performed on the overlapping genes to visualize the level of similarity between the different groups, using Euclidean distance as the distance measure and complete linkage clustering as the clustering method.

Pathway enrichment analysis. Gene set enrichment analysis (GSEA) (124) preranked with 1,000 permutations using the Hallmark gene sets (125), transcription factor targets (C3) from Molecular Signatures Database version 5.0 (MSigDB), was performed on the genes differentially expressed between comparisons. The differentially expressed genes were preranked by the decreasing order of their –log(*P* value) times their sign(log fold change) or sign(correlation coefficient) to identify pathways upregulated and downregulated or pathways correlated with HIV msRNA measured by TILDA. The obtained *P* values of the pathways were corrected for multiple comparisons using the BH method. Pathways at a nominal and adjusted *P* value of <0.05 were considered significant.

For the HDAC gene sets, we used the Pathway Interaction Database (PID) HDAC class I/II/III gene sets, and we built a custom gene set that included known (from the literature) histone deacetylases, histone acetyltransferases, and other chromatin-modifying/modeling enzymes (PubMed identifier, 29236683).

Sample-level enrichment analysis (SLEA) (126) was used to represent the expression of pathways by calculating the z-score of the pathway per sample. The mean expression value of genes of the significant gene sets was compared to the mean expression of 1,000 random gene sets of the same size as the selected gene set for every sample. The difference between the observed and expected mean expression values for each gene set was calculated.

Statistical analysis. A paired Wilcoxon rank sum test was performed to compare paired samples, and the obtained *P* values were corrected for multiple comparisons using the BH method. All *P* values at a nominal and adjusted *P* value of <0.05 were considered significant.

Multivariate model of activation markers that best predict the frequency of cells expressing inducible HIV msRNA. Feature selection was performed using the least absolute shrinkage and selection operator (LASSO) (51) technique, in order to determine the activation markers expressed by memory subsets that best predicted the induction of HIV msRNA. The model was optimized using leave-one-out cross-validation, and the least cross-validated mean square error (MSE) was determined.

Data availability. All materials are available upon request from the authors, subject to completion of a material transfer agreement.

SUPPLEMENTAL MATERIAL

Supplemental material for this article may be found at https://doi.org/10.1128/JVI.00969-19.

SUPPLEMENTAL FILE 1, XLSX file, 0.01 MB.
SUPPLEMENTAL FILE 2, XLSX file, 0.01 MB.
SUPPLEMENTAL FILE 3, XLSX file, 0.02 MB.
SUPPLEMENTAL FILE 4, XLSX file, 0.01 MB.
SUPPLEMENTAL FILE 5, XLSX file, 0.02 MB.
SUPPLEMENTAL FILE 6, XLSX file, 0.01 MB.
SUPPLEMENTAL FILE 7, PDF file, 0.6 MB.

ACKNOWLEDGMENTS

We thank Mirko Paiardini for critical reading of the manuscript and Rebecca Hoh for clinical data support. The following reagents were obtained through the NIH AIDS Reagent Program, Division of AIDS, NIAID, NIH: raltegravir (catalog number 11680) from Merck & Co., Inc., Kenilworth, NJ, USA, and p89.6 from Ronald G. Collman.

The research was supported by a grant from Merck Sharp and Dohme Corp., a

subsidiary of Merck & Co., Inc., Kenilworth, NJ, USA, and NIH grant AI-110334. D.A.K. and A.-G.B.-B. were additionally funded through a University of Miami Center for AIDS Research Developmental Award. R.B., M.M., and D.H. are all employees of Merck Sharp & Dohme Corp., a subsidiary of Merck & Co., Inc., Kenilworth, NJ, USA. S.Y. is an employee of Janssen Pharmaceuticals. J.H.B. is an employee of ViiV Healthcare.

D.A.K. designed and performed the experiments, analyzed the data, and wrote the manuscript. S.Y., S.P.R., J.H.B., and A.-G.B.-B. performed the experiments. A.T. performed statistical analysis and analysis of RNA sequencing data and contributed to the writing of the manuscript. R.B., M.M., and D.H. designed the experiments. S.G.D. provided patient samples and contributed to the writing of the manuscript. N.C. and R.-P. S. designed the experiments and contributed to the writing of the manuscript.

REFERENCES

1. Chomont N, El-Far M, Ancuta P, Trautmann L, Procopio FA, Yassine-Diab B, Boucher G, Boulassel MR, Ghattas G, Brenchley JM, Schacker TW, Hill BJ, Douek DC, Routy JP, Haddad EK, Sékaly RP. 2009. HIV reservoir size and persistence are driven by T cell survival and homeostatic proliferation. Nat Med 15:893–900. https://doi.org/10.1038/nm.1972.
2. Bacchus C, Cheret A, Avettand-Fenoel V, Nembot G, Melard A, Blanc C, Lascoux-Combe C, Slama L, Allegre T, Allavena C, Yazdanpanah Y, Duvivier C, Katlama C, Goujard C, Seksik BC, Leplatois A, Molina JM, Meyer L, Autran B, Rouzioux C, OPTIPRIM ANRS 147 Study Group. 2013. A single HIV-1 cluster and a skewed immune homeostasis drive the early spread of HIV among resting CD4+ cell subsets within one month post-infection. PLoS One 8:e64219. https://doi.org/10.1371/journal.pone.0064219.
3. Chomont N, DaFonseca S, Vandergeeten C, Ancuta P, Sekaly RP. 2011. Maintenance of CD4+ T-cell memory and HIV persistence: keeping memory, keeping HIV. Curr Opin HIV AIDS 6:30–36. https://doi.org/10.1097/COH.0b013e3283413775.
4. Yukl SA, Shergill AK, Ho T, Killian M, Girling V, Epling L, Li P, Wong LK, Crouch P, Deeks SG, Havlir DV, McQuaid K, Sinclair E, Wong JK. 2013. The distribution of HIV DNA and RNA in cell subsets differs in gut and blood of HIV-positive patients on ART: implications for viral persistence. J Infect Dis 208:1212–1220. https://doi.org/10.1093/infdis/jit308.
5. Buzon MJ, Sun H, Li C, Shaw A, Seiss K, Ouyang Z, Martin-Gayo E, Leng J, Henrich TJ, Li JZ, Pereyra F, Zurakowski R, Walker BD, Rosenberg ES, Yu XG, Lichterfeld M. 2014. HIV-1 persistence in CD4+ T cells with stem cell-like properties. Nat Med 20:139–142. https://doi.org/10.1038/nm.3445.
6. Saez-Cirion A, Bacchus C, Hocqueloux L, Avettand-Fenoel V, Girault I, Lecuroux C, Potard V, Versmisse P, Melard A, Prazuck T, Descours B, Guergnon J, Viard JP, Boufassa F, Lambotte O, Goujard C, Meyer L, Costagliola D, Venet A, Pancino G, Autran B, Rouzioux C, ANRS VISCONTI Study Group. 2013. Post-treatment HIV-1 controllers with a long-term virological remission after the interruption of early initiated antiretroviral therapy ANRS VISCONTI Study. PLoS Pathog 9:e1003211. https://doi.org/10.1371/journal.ppat.1003211.
7. Cyster JG. 2005. Chemokines, sphingosine-1-phosphate, and cell migration in secondary lymphoid organs. Annu Rev Immunol 23:127–159. https://doi.org/10.1146/annurev.immunol.23.021704.115628.
8. Pepper M, Jenkins MK. 2011. Origins of CD4(+) effector and central memory T cells. Nat Immunol 12:467–471. https://doi.org/10.1038/ni.2038.
9. Fas SC, Baumann S, Krueger A, Frey CR, Schulze-Bergkamen H, Brenner D, Stumpf C, Kappes K, Krammer PH. 2006. In vitro generated human memory-like T cells are CD95 type II cells and resistant towards CD95-mediated apoptosis. Eur J Immunol 36:2894–2903. https://doi.org/10.1002/eji.200635925.
10. Inaba M, Kurasawa K, Mamura M, Kumano K, Saito Y, Iwamoto I. 1999. Primed T cells are more resistant to Fas-mediated activation-induced cell death than naive T cells. J Immunol 163:1315–1320.
11. Desbarats J, Wade T, Wade WF, Newell MK. 1999. Dichotomy between naive and memory CD4(+) T cell responses to Fas engagement. Proc Natl Acad Sci U S A 96:8104–8109. https://doi.org/10.1073/pnas.96.14.8104.
12. Yin Y, Zhang S, Luo H, Zhang X, Geng G, Li J, Guo X, Cai W, Li L, Liu C, Zhang H. 2015. Interleukin 7 up-regulates CD95 protein on CD4+ T cells by affecting mRNA alternative splicing: priming for a synergistic effect on HIV-1 reservoir maintenance. J Biol Chem 290:35–45. https://doi.org/10.1074/jbc.M114.598631.
13. Riou C, Yassine-Diab B, Van Grevenynghe J, Somogyi R, Greller LD, Gagnon D, Gimmig S, Wilkinson P, Shi Y, Cameron MJ, Campos-Gonzalez R, Balderas RS, Kelvin D, Sekaly RP, Haddad EK. 2007. Convergence of TCR and cytokine signaling leads to FOXO3a phosphorylation and drives the survival of CD4+ central memory T cells. J Exp Med 204:79–91. https://doi.org/10.1084/jem.20061681.
14. Macallan DC, Wallace D, Zhang Y, De Lara C, Worth AT, Ghattas H, Griffin GE, Beverley PC, Tough DF. 2004. Rapid turnover of effector-memory CD4(+) T cells in healthy humans. J Exp Med 200:255–260. https://doi.org/10.1084/jem.20040341.
15. Fritsch RD, Shen X, Sims GP, Hathcock KS, Hodes RJ, Lipsky PE. 2005. Stepwise differentiation of CD4 memory T cells defined by expression of CCR7 and CD27. J Immunol 175:6489–6497. https://doi.org/10.4049/jimmunol.175.10.6489.
16. Okada R, Kondo T, Matsuki F, Takata H, Takiguchi M. 2008. Phenotypic classification of human CD4+ T cell subsets and their differentiation. Int Immunol 20:1189–1199. https://doi.org/10.1093/intimm/dxn075.
17. Picker LJ, Reed-Inderbitzin EF, Hagen SI, Edgar JB, Hansen SG, Legasse A, Planer S, Piatak M, Jr, Lifson JD, Maino VC, Axthelm MK, Villinger F. 2006. IL-15 induces CD4 effector memory T cell production and tissue emigration in nonhuman primates. J Clin Invest 116:1514–1524. https://doi.org/10.1172/JCI27564.
18. Lugli E, Goldman CK, Perera LP, Smedley J, Pung R, Yovandich JL, Creekmore SP, Waldmann TA, Roederer M. 2010. Transient and persistent effects of IL-15 on lymphocyte homeostasis in nonhuman primates. Blood 116:3238–3248. https://doi.org/10.1182/blood-2010-03-275438.
19. Abdelsamed HA, Moustaki A, Fan Y, Dogra P, Ghoneim HE, Zebley CC, Triplett BM, Sekaly RP, Youngblood B. 2017. Human memory CD8 T cell effector potential is epigenetically preserved during in vivo homeostasis. J Exp Med 214:1593–1606. https://doi.org/10.1084/jem.20161760.
20. Messi M, Giacchetto I, Nagata K, Lanzavecchia A, Natoli G, Sallusto F. 2003. Memory and flexibility of cytokine gene expression as separable properties of human T(H)1 and T(H)2 lymphocytes. Nat Immunol 4:78–86. https://doi.org/10.1038/ni872.
21. Lees JR, Farber DL. 2010. Generation, persistence and plasticity of CD4 T-cell memories. Immunology 130:463–470. https://doi.org/10.1111/j.1365-2567.2010.03288.x.
22. Fromentin R, Bakeman W, Lawani MB, Khoury G, Hartogensis W, DaFonseca S, Killian M, Epling L, Hoh R, Sinclair E, Hecht FM, Bacchetti P, Deeks SG, Lewin SR, Sekaly RP, Chomont N. 2016. CD4+ T cells expressing PD-1, TIGIT and LAG-3 contribute to HIV persistence during ART. PLoS Pathog 12:e1005761. https://doi.org/10.1371/journal.ppat.1005761.
23. Descours B, Avettand-Fenoel V, Blanc C, Samri A, Melard A, Supervie V, Theodorou I, Carcelain G, Rouzioux C, Autran B, ALT ANRS CO15 Study Group. 2012. Immune responses driven by protective human leukocyte antigen alleles from long-term nonprogressors are associated with low HIV reservoir in central memory CD4 T cells. Clin Infect Dis 54:1495–1503. https://doi.org/10.1093/cid/cis188.
24. Hiener B, Horsburgh BA, Eden JS, Barton K, Schlub TE, Lee E, von Stockenstrom S, Odevall L, Milush JM, Liegler T, Sinclair E, Hoh R, Boritz

EA, Douek D, Fromentin R, Chomont N, Deeks SG, Hecht FM, Palmer S. 2017. Identification of genetically intact HIV-1 proviruses in specific CD4+ T cells from effectively treated participants. Cell Rep 21:813–822. https://doi.org/10.1016/j.celrep.2017.09.081.
25. Deeks SG. 2012. HIV: shock and kill. Nature 487:439–440. https://doi.org/10.1038/487439a.
26. Vandergeeten C, Fromentin R, Merlini E, Lawani MB, DaFonseca S, Bakeman W, McNulty A, Ramgopal M, Michael N, Kim JH, Ananworanich J, Chomont N. 2014. Cross-clade ultrasensitive PCR-based assays to measure HIV persistence in large-cohort studies. J Virol 88:12385–12396. https://doi.org/10.1128/JVI.00609-14.
27. Procopio FA, Fromentin R, Kulpa DA, Brehm JH, Bebin A-G, Strain MC, Richman DD, O'Doherty U, Palmer S, Hecht FM, Hoh R, Barnard RJO, Miller MD, Hazuda DJ, Deeks SG, Sékaly R-P, Chomont N. 2015. A novel assay to measure the magnitude of the inducible viral reservoir in HIV-infected individuals. EBioMedicine 2:874–883. https://doi.org/10.1016/j.ebiom.2015.06.019.
28. Ramaswamy M, Cruz AC, Cleland SY, Deng M, Price S, Rao VK, Siegel RM. 2011. Specific elimination of effector memory CD4+ T cells due to enhanced Fas signaling complex formation and association with lipid raft microdomains. Cell Death Differ 18:712–720. https://doi.org/10.1038/cdd.2010.155.
29. Tiemessen MM, Kunzmann S, Schmidt-Weber CB, Garssen J, Bruijnzeel-Koomen CA, Knol EF, van Hoffen E. 2003. Transforming growth factor-beta inhibits human antigen-specific CD4+ T cell proliferation without modulating the cytokine response. Int Immunol 15:1495–1504. https://doi.org/10.1093/intimm/dxg147.
30. Takahashi H, Tatsumi M, Matsuda M, Nagashima K, Kurata T, Hall WW. 1997. The role of topoisomerase I in HIV-1 replication. Leukemia 11(Suppl 3):26–28.
31. Kondapi AK, Satyanarayana N, Saikrishna AD. 2006. A study of the topoisomerase II activity in HIV-1 replication using the ferrocene derivatives as probes. Arch Biochem Biophys 450:123–132. https://doi.org/10.1016/j.abb.2006.04.003.
32. Shoya Y, Tokunaga K, Sawa H, Maeda M, Ueno T, Yoshikawa T, Hasegawa H, Sata T, Kurata T, Hall WW, Cullen BR, Takahashi H. 2003. Human topoisomerase I promotes HIV-1 proviral DNA synthesis: implications for the species specificity and cellular tropism of HIV-1 infection. Proc Natl Acad Sci U S A 100:8442–8447. https://doi.org/10.1073/pnas.1430827100.
33. Guerrero S, Batisse J, Libre C, Bernacchi S, Marquet R, Paillart JC. 2015. HIV-1 replication and the cellular eukaryotic translation apparatus. Viruses 7:199–218. https://doi.org/10.3390/v7010199.
34. Moran ST, Haider K, Ow Y, Milton P, Chen L, Pillai S. 2003. Protein kinase C-associated kinase can activate NFkappaB in both a kinase-dependent and a kinase-independent manner. J Biol Chem 278:21526–21533. https://doi.org/10.1074/jbc.M301575200.
35. Muto A, Ruland J, McAllister-Lucas LM, Lucas PC, Yamaoka S, Chen FF, Lin A, Mak TW, Núñez G, Inohara N. 2002. Protein kinase C-associated kinase (PKK) mediates BclX-independent NF-kappa B activation induced by phorbol ester. J Biol Chem 277:31871–31876. https://doi.org/10.1074/jbc.M202222200.
36. Chan JK, Greene WC. 2011. NF-kappaB/Rel: agonist and antagonist roles in HIV-1 latency. Curr Opin HIV AIDS 6:12–18. https://doi.org/10.1097/COH.0b013e32834124fd.
37. Duverger A, Wolschendorf F, Anderson JC, Wagner F, Bosque A, Shishido T, Jones J, Planelles V, Willey C, Cron RQ, Kutsch O. 2014. Kinase control of latent HIV-1 infection: PIM-1 kinase as a major contributor to HIV-1 reactivation. J Virol 88:364–376. https://doi.org/10.1128/JVI.02682-13.
38. Kim MV, Ouyang W, Liao W, Zhang MQ, Li MO. 2013. The transcription factor Foxo1 controls central-memory CD8+ T cell responses to infection. Immunity 39:286–297. https://doi.org/10.1016/j.immuni.2013.07.013.
39. Hedrick SM, Hess Michelini R, Doedens AL, Goldrath AW, Stone EL. 2012. FOXO transcription factors throughout T cell biology. Nat Rev Immunol 12:649–661. https://doi.org/10.1038/nri3278.
40. Dejean AS, Hedrick SM, Kerdiles YM. 2011. Highly specialized role of Forkhead box O transcription factors in the immune system. Antioxid Redox Signal 14:663–674. https://doi.org/10.1089/ars.2010.3414.
41. Coffer PJ, Burgering BM. 2004. Forkhead-box transcription factors and their role in the immune system. Nat Rev Immunol 4:889–899. https://doi.org/10.1038/nri1488.
42. Klase Z, Yedavalli VS, Houzet L, Perkins M, Maldarelli F, Brenchley J, Strebel K, Liu P, Jeang KT. 2014. Activation of HIV-1 from latent infection via synergy of RUNX1 inhibitor Ro5-3335 and SAHA. PLoS Pathog 10:e1003997. https://doi.org/10.1371/journal.ppat.1003997.
43. Murphy KM, Stockinger B. 2010. Effector T cell plasticity: flexibility in the face of changing circumstances. Nat Immunol 11:674–680. https://doi.org/10.1038/ni.1899.
44. Yang CY, Best JA, Knell J, Yang E, Sheridan AD, Jesionek AK, Li HS, Rivera RR, Lind KC, D'Cruz LM, Watowich SS, Murre C, Goldrath AW. 2011. The transcriptional regulators Id2 and Id3 control the formation of distinct memory CD8+ T cell subsets. Nat Immunol 12:1221–1229. https://doi.org/10.1038/ni.2158.
45. Kaech SM, Tan JT, Wherry EJ, Konieczny BT, Surh CD, Ahmed R. 2003. Selective expression of the interleukin 7 receptor identifies effector CD8 T cells that give rise to long-lived memory cells. Nat Immunol 4:1191–1198. https://doi.org/10.1038/ni1009.
46. Schluns KS, Kieper WC, Jameson SC, Lefrancois L. 2000. Interleukin-7 mediates the homeostasis of naive and memory CD8 T cells in vivo. Nat Immunol 1:426–432. https://doi.org/10.1038/80868.
47. Tan JT, Dudl E, LeRoy E, Murray R, Sprent J, Weinberg KI, Surh CD. 2001. IL-7 is critical for homeostatic proliferation and survival of naive T cells. Proc Natl Acad Sci U S A 98:8732–8737. https://doi.org/10.1073/pnas.161126098.
48. Fuller MJ, Hildeman DA, Sabbaj S, Gaddis DE, Tebo AE, Shang L, Goepfert PA, Zajac AJ. 2005. Cutting edge: emergence of CD127high functionally competent memory T cells is compromised by high viral loads and inadequate T cell help. J Immunol 174:5926–5930. https://doi.org/10.4049/jimmunol.174.10.5926.
49. Lang KS, Recher M, Navarini AA, Harris NL, Lohning M, Junt T, Probst HC, Hengartner H, Zinkernagel RM. 2005. Inverse correlation between IL-7 receptor expression and CD8 T cell exhaustion during persistent antigen stimulation. Eur J Immunol 35:738–745. https://doi.org/10.1002/eji.200425828.
50. Ma A, Koka R, Burkett P. 2006. Diverse functions of IL-2, IL-15, and IL-7 in lymphoid homeostasis. Annu Rev Immunol 24:657–679. https://doi.org/10.1146/annurev.immunol.24.021605.090727.
51. Tibshirani R. 1996. Regression shrinkage and selection via the Lasso. J R Stat Soc Series B Stat Methodol 58:267–288. https://doi.org/10.1111/j.2517-6161.1996.tb02080.x.
52. Blankson JN, Persaud D, Siliciano RF. 2002. The challenge of viral reservoirs in HIV-1 infection. Annu Rev Med 53:557–593. https://doi.org/10.1146/annurev.med.53.082901.104024.
53. Pierson T, McArthur J, Siliciano RF. 2000. Reservoirs for HIV-1: mechanisms for viral persistence in the presence of antiviral immune responses and antiretroviral therapy. Annu Rev Immunol 18:665–708. https://doi.org/10.1146/annurev.immunol.18.1.665.
54. Bauer I, Grozio A, Lasiglie D, Basile G, Sturla L, Magnone M, Sociali G, Soncini D, Caffa I, Poggi A, Zoppoli G, Cea M, Feldmann G, Mostoslavsky R, Ballestrero A, Patrone F, Bruzzone S, Nencioni A. 2012. The NAD+-dependent histone deacetylase SIRT6 promotes cytokine production and migration in pancreatic cancer cells by regulating Ca2+ responses. J Biol Chem 287:40924–40937. https://doi.org/10.1074/jbc.M112.405837.
55. Finkel T, Deng CX, Mostoslavsky R. 2009. Recent progress in the biology and physiology of sirtuins. Nature 460:587–591. https://doi.org/10.1038/nature08197.
56. Parbin S, Kar S, Shilpi A, Sengupta D, Deb M, Rath SK, Patra SK. 2014. Histone deacetylases: a saga of perturbed acetylation homeostasis in cancer. J Histochem Cytochem 62:11–33. https://doi.org/10.1369/0022155413506582.
57. Seto E, Yoshida M. 2014. Erasers of histone acetylation: the histone deacetylase enzymes. Cold Spring Harb Perspect Biol 6:a018713. https://doi.org/10.1101/cshperspect.a018713.
58. Kwon HS, Brent MM, Getachew R, Jayakumar P, Chen LF, Schnolzer M, McBurney MW, Marmorstein R, Greene WC, Ott M. 2008. Human immunodeficiency virus type 1 Tat protein inhibits the SIRT1 deacetylase and induces T cell hyperactivation. Cell Host Microbe 3:158–167. https://doi.org/10.1016/j.chom.2008.02.002.
59. Tang X, Shi L, Xie N, Liu Z, Qian M, Meng F, Xu Q, Zhou M, Cao X, Zhu WG, Liu B. 2017. SIRT7 antagonizes TGF-beta signaling and inhibits breast cancer metastasis. Nat Commun 8:318. https://doi.org/10.1038/s41467-017-00396-9.
60. Sarikhani M, Maity S, Mishra S, Jain A, Tamta AK, Ravi V, Kondapalli MS, Desingu PA, Khan D, Kumar S, Rao S, Inbaraj M, Pandit AS, Sundaresan NR. 2018. SIRT2 deacetylase represses NFAT transcription factor to

maintain cardiac homeostasis. J Biol Chem 293:5281–5294. https://doi.org/10.1074/jbc.RA117.000915.
61. Wapenaar H, Dekker FJ. 2016. Histone acetyltransferases: challenges in targeting bi-substrate enzymes. Clin Epigenetics 8:59. https://doi.org/10.1186/s13148-016-0225-2.
62. Rother MB, van Attikum H. 2017. DNA repair goes hip-hop: SMARCA and CHD chromatin remodellers join the break dance. Philos Trans R Soc Lond B Biol Sci 372:20160285. https://doi.org/10.1098/rstb.2016.0285.
63. Flaus A, Owen-Hughes T. 2011. Mechanisms for ATP-dependent chromatin remodelling: the means to the end. FEBS J 278:3579–3595. https://doi.org/10.1111/j.1742-4658.2011.08281.x.
64. Margolis DM. 2011. Histone deacetylase inhibitors and HIV latency. Curr Opin HIV AIDS 6:25–29. https://doi.org/10.1097/COH.0b013e328341242d.
65. Battistini A, Sgarbanti M. 2014. HIV-1 latency: an update of molecular mechanisms and therapeutic strategies. Viruses 6:1715–1758. https://doi.org/10.3390/v6041715.
66. Kehrl JH, Wakefield LM, Roberts AB, Jakowlew S, Alvarez-Mon M, Derynck R, Sporn MB, Fauci AS. 1986. Production of transforming growth factor beta by human T lymphocytes and its potential role in the regulation of T cell growth. J Exp Med 163:1037–1050. https://doi.org/10.1084/jem.163.5.1037.
67. Letterio JJ, Roberts AB. 1998. Regulation of immune responses by TGF-beta. Annu Rev Immunol 16:137–161. https://doi.org/10.1146/annurev.immunol.16.1.137.
68. Zhang X, Giangreco L, Broome HE, Dargan CM, Swain SL. 1995. Control of CD4 effector fate: transforming growth factor beta 1 and interleukin 2 synergize to prevent apoptosis and promote effector expansion. J Exp Med 182:699–709. https://doi.org/10.1084/jem.182.3.699.
69. Cerwenka A, Kovar H, Majdic O, Holter W. 1996. Fas- and activation-induced apoptosis are reduced in human T cells preactivated in the presence of TGF-beta 1. J Immunol 156:459–464.
70. Wang FX, Xu Y, Sullivan J, Souder E, Argyris EG, Acheampong EA, Fisher J, Sierra M, Thomson MM, Najera R, Frank I, Kulkosky J, Pomerantz RJ, Nunnari G. 2005. IL-7 is a potent and proviral strain-specific inducer of latent HIV-1 cellular reservoirs of infected individuals on virally suppressive HAART. J Clin Invest 115:128–137. https://doi.org/10.1172/JCI22574.
71. Vandergeeten C, Fromentin R, DaFonseca S, Lawani MB, Sereti I, Lederman MM, Ramgopal M, Routy JP, Sékaly RP, Chomont N. 2013. Interleukin-7 promotes HIV persistence during antiretroviral therapy. Blood 121:4321–4329. https://doi.org/10.1182/blood-2012-11-465625.
72. Sahu GK, Lee K, Ji J, Braciale V, Baron S, Cloyd MW. 2006. A novel in vitro system to generate and study latently HIV-infected long-lived normal CD4+ T-lymphocytes. Virology 355:127–137. https://doi.org/10.1016/j.virol.2006.07.020.
73. Tyagi M, Pearson RJ, Karn J. 2010. Establishment of HIV latency in primary CD4+ cells is due to epigenetic transcriptional silencing and P-TEFb restriction. J Virol 84:6425–6437. https://doi.org/10.1128/JVI.01519-09.
74. Khattar M, Miyahara Y, Schroder PM, Xie A, Chen W, Stepkowski SM. 2014. Interleukin-21 is a critical regulator of CD4 and CD8 T cell survival during priming under interleukin-2 deprivation conditions. PLoS One 9:e85882. https://doi.org/10.1371/journal.pone.0085882.
75. Flavell RA, Sanjabi S, Wrzesinski SH, Licona-Limón P. 2010. The polarization of immune cells in the tumour environment by TGFbeta. Nat Rev Immunol 10:554–567. https://doi.org/10.1038/nri2808.
76. Tu E, Chia PZ, Chen W. 2014. TGFbeta in T cell biology and tumor immunity: angel or devil? Cytokine Growth Factor Rev 25:423–435. https://doi.org/10.1016/j.cytogfr.2014.07.014.
77. Banga R, Procopio FA, Cavassini M, Perreau M. 2016. In vitro reactivation of replication-competent and infectious HIV-1 by histone deacetylase inhibitors. J Virol 90:1858–1871. https://doi.org/10.1128/JVI.02359-15.
78. Darcis G, Kula A, Bouchat S, Fujinaga K, Corazza F, Ait-Ammar A, Delacourt N, Melard A, Kabeya K, Vanhulle C, Van Driessche B, Gatot JS, Cherrier T, Pianowski LF, Gama L, Schwartz C, Vila J, Burny A, Clumeck N, Moutschen M, De Wit S, Peterlin BM, Rouzioux C, Rohr O, Van Lint C. 2015. An in-depth comparison of latency-reversing agent combinations in various in vitro and ex vivo HIV-1 latency models identified bryostatin-1+JQ1 and ingenol-B+JQ1 to potently reactivate viral gene expression. PLoS Pathog 11:e1005063. https://doi.org/10.1371/journal.ppat.1005063.
79. Bullen CK, Laird GM, Durand CM, Siliciano JD, Siliciano RF. 2014. New ex vivo approaches distinguish effective and ineffective single agents for reversing HIV-1 latency in vivo. Nat Med 20:425–429. https://doi.org/10.1038/nm.3489.
80. Spina CA, Anderson J, Archin NM, Bosque A, Chan J, Famiglietti M, Greene WC, Kashuba A, Lewin SR, Margolis DM, Mau M, Ruelas D, Saleh S, Shirakawa K, Siliciano RF, Singhania A, Soto PC, Terry VH, Verdin E, Woelk C, Wooden S, Xing S, Planelles V. 2013. An in-depth comparison of latent HIV-1 reactivation in multiple cell model systems and resting CD4+ T cells from aviremic patients. PLoS Pathog 9:e1003834. https://doi.org/10.1371/journal.ppat.1003834.
81. Curiel RE, Garcia CS, Farooq L, Aguero MF, Espinoza-Delgado I. 2001. Bryostatin-1 and IL-2 synergize to induce IFN-gamma expression in human peripheral blood T cells: implications for cancer immunotherapy. J Immunol 167:4828–4837. https://doi.org/10.4049/jimmunol.167.9.4828.
82. Marks PA, Richon VM, Rifkind RA. 2000. Histone deacetylase inhibitors: inducers of differentiation or apoptosis of transformed cells. J Natl Cancer Inst 92:1210–1216. https://doi.org/10.1093/jnci/92.15.1210.
83. Wood MD, Hiura H, Tunster SJ, Arima T, Shin JY, Higgins MJ, John RM. 2010. Autonomous silencing of the imprinted Cdkn1c gene in stem cells. Epigenetics 5:214–221. https://doi.org/10.4161/epi.5.3.11275.
84. Nabel G, Baltimore D. 1987. An inducible transcription factor activates expression of human immunodeficiency virus in T cells. Nature 326:711–713. https://doi.org/10.1038/326711a0.
85. Tong-Starksen SE, Luciw PA, Peterlin BM. 1987. Human immunodeficiency virus long terminal repeat responds to T-cell activation signals. Proc Natl Acad Sci U S A 84:6845–6849. https://doi.org/10.1073/pnas.84.19.6845.
86. Duh EJ, Maury WJ, Folks TM, Fauci AS, Rabson AB. 1989. Tumor necrosis factor alpha activates human immunodeficiency virus type 1 through induction of nuclear factor binding to the NF-kappa B sites in the long terminal repeat. Proc Natl Acad Sci U S A 86:5974–5978. https://doi.org/10.1073/pnas.86.15.5974.
87. Rabson AB, Lin HC. 2000. NF-kappa B and HIV: linking viral and immune activation. Adv Pharmacol 48:161–207. https://doi.org/10.1016/S1054-3589(00)48006-3.
88. Hess Michelini R, Doedens AL, Goldrath AW, Hedrick SM. 2013. Differentiation of CD8 memory T cells depends on Foxo1. J Exp Med 210:1189–1200. https://doi.org/10.1084/jem.20130392.
89. Archin NM, Kirchherr JL, Sung JA, Clutton G, Sholtis K, Xu Y, Allard B, Stuelke E, Kashuba AD, Kuruc JD, Eron J, Gay CL, Goonetilleke N, Margolis DM. 2017. Interval dosing with the HDAC inhibitor vorinostat effectively reverses HIV latency. J Clin Invest 127:3126–3135. https://doi.org/10.1172/JCI92684.
90. Archin NM, Liberty AL, Kashuba AD, Choudhary SK, Kuruc JD, Crooks AM, Parker DC, Anderson EM, Kearney MF, Strain MC, Richman DD, Hudgens MG, Bosch RJ, Coffin JM, Eron JJ, Hazuda DJ, Margolis DM. 2012. Administration of vorinostat disrupts HIV-1 latency in patients on antiretroviral therapy. Nature 487:482–485. https://doi.org/10.1038/nature11286.
91. Vukmanovic-Stejic M, Zhang Y, Cook JE, Fletcher JM, McQuaid A, Masters JE, Rustin MH, Taams LS, Beverley PC, Macallan DC, Akbar AN. 2006. Human CD4+ CD25hi Foxp3+ regulatory T cells are derived by rapid turnover of memory populations in vivo. J Clin Invest 116:2423–2433. https://doi.org/10.1172/JCI28941.
92. Farber DL, Yudanin NA, Restifo NP. 2014. Human memory T cells: generation, compartmentalization and homeostasis. Nat Rev Immunol 14:24–35. https://doi.org/10.1038/nri3567.
93. Liu J, Roederer M. 2007. Differential susceptibility of leukocyte subsets to cytotoxic T cell killing: implications for HIV immunopathogenesis. Cytometry A 71:94–104. https://doi.org/10.1002/cyto.a.20363.
94. Buzon MJ, Yang Y, Ouyang Z, Sun H, Seiss K, Rogich J, Le Gall S, Pereyra F, Rosenberg ES, Yu XG, Lichterfeld M. 2014. Susceptibility to CD8 T-cell-mediated killing influences the reservoir of latently HIV-1-infected CD4 T cells. J Acquir Immune Defic Syndr 65:1–9. https://doi.org/10.1097/QAI.0b013e3182a1bc81.
95. Wonderlich ER, Leonard JA, Collins KL. 2011. HIV immune evasion disruption of antigen presentation by the HIV Nef protein. Adv Virus Res 80:103–127. https://doi.org/10.1016/B978-0-12-385987-7.00005-1.
96. Kirchhoff F. 2010. Immune evasion and counteraction of restriction factors by HIV-1 and other primate lentiviruses. Cell Host Microbe 8:55–67. https://doi.org/10.1016/j.chom.2010.06.004.
97. Johnson WE, Desrosiers RC. 2002. Viral persistence: HIV's strategies of immune system evasion. Annu Rev Med 53:499–518. https://doi.org/10.1146/annurev.med.53.082901.104053.

98. Collins KL, Chen BK, Kalams SA, Walker BD, Baltimore D. 1998. HIV-1 Nef protein protects infected primary cells against killing by cytotoxic T lymphocytes. Nature 391:397–401. https://doi.org/10.1038/34929.
99. Poon B, Grovit-Ferbas K, Stewart SA, Chen IS. 1998. Cell cycle arrest by Vpr in HIV-1 virions and insensitivity to antiretroviral agents. Science 281:266–269. https://doi.org/10.1126/science.281.5374.266.
100. Rice AP, Kimata JT. 2015. Subversion of cell cycle regulatory mechanisms by HIV. Cell Host Microbe 17:736–740. https://doi.org/10.1016/j.chom.2015.05.010.
101. Newfeld SJ, Wisotzkey RG, Kumar S. 1999. Molecular evolution of a developmental pathway: phylogenetic analyses of transforming growth factor-beta family ligands, receptors and Smad signal transducers. Genetics 152:783–795.
102. Schmierer B, Hill CS. 2007. TGFbeta-SMAD signal transduction: molecular specificity and functional flexibility. Nat Rev Mol Cell Biol 8:970–982. https://doi.org/10.1038/nrm2297.
103. Barouch DH, Ghneim K, Bosche WJ, Li Y, Berkemeier B, Hull M, Bhattacharyya S, Cameron M, Liu J, Smith K, Borducchi E, Cabral C, Peter L, Brinkman A, Shetty M, Li H, Gittens C, Baker C, Wagner W, Lewis MG, Colantonio A, Kang HJ, Li W, Lifson JD, Piatak M, Sekaly RP. 2016. Rapid inflammasome activation following mucosal SIV infection of rhesus monkeys. Cell 165:656–667. https://doi.org/10.1016/j.cell.2016.03.021.
104. He T, Brocca-Cofano E, Policicchio BB, Sivanandham R, Gautam R, Raehtz KD, Xu C, Pandrea I, Apetrei C. 2016. Cutting edge: T regulatory cell depletion reactivates latent simian immunodeficiency virus (SIV) in controller macaques while boosting SIV-specific T lymphocytes. J Immunol 197:4535–4539. https://doi.org/10.4049/jimmunol.1601539.
105. Boise LH, Minn AJ, June CH, Lindsten T, Thompson CB. 1995. Growth factors can enhance lymphocyte survival without committing the cell to undergo cell division. Proc Natl Acad Sci U S A 92:5491–5495. https://doi.org/10.1073/pnas.92.12.5491.
106. Vella A, Teague TK, Ihle J, Kappler J, Marrack P. 1997. Interleukin 4 (IL-4) or IL-7 prevents the death of resting T cells: stat6 is probably not required for the effect of IL-4. J Exp Med 186:325–330. https://doi.org/10.1084/jem.186.2.325.
107. Vella AT, Dow S, Potter TA, Kappler J, Marrack P. 1998. Cytokine-induced survival of activated T cells in vitro and in vivo. Proc Natl Acad Sci U S A 95:3810–3815. https://doi.org/10.1073/pnas.95.7.3810.
108. Coiras M, Bermejo M, Descours B, Mateos E, García-Pérez J, López-Huertas MR, Lederman MM, Benkirane M, Alcamí J. 2016. IL-7 induces SAMHD1 phosphorylation in CD4+ T Lymphocytes, improving early steps of HIV-1 life cycle. Cell Rep 14:2100–2107. https://doi.org/10.1016/j.celrep.2016.02.022.
109. Wang Z, Gurule EE, Brennan TP, Gerold JM, Kwon KJ, Hosmane NN, Kumar MR, Beg SA, Capoferri AA, Ray SC, Ho YC, Hill AL, Siliciano JD, Siliciano RF. 2018. Expanded cellular clones carrying replication-competent HIV-1 persist, wax, and wane. Proc Natl Acad Sci U S A 115:E2575–E2584. https://doi.org/10.1073/pnas.1720665115.
110. Ebert EC. 1999. Inhibitory effects of transforming growth factor-beta (TGF-beta) on certain functions of intraepithelial lymphocytes. Clin Exp Immunol 115:415–420. https://doi.org/10.1046/j.1365-2249.1999.00824.x.
111. Nijhuis EW, Vd Wiel-van Kemenade E, Figdor CG, van Lier RA. 1990. Activation and expansion of tumour-infiltrating lymphocytes by anti-CD3 and anti-CD28 monoclonal antibodies. Cancer Immunol Immunother 32:245–250. https://doi.org/10.1007/bf01741708.
112. Jung G, Ledbetter JA, Muller-Eberhard HJ. 1987. Induction of cytotoxicity in resting human T lymphocytes bound to tumor cells by antibody heteroconjugates. Proc Natl Acad Sci U S A 84:4611–4615. https://doi.org/10.1073/pnas.84.13.4611.
113. Collman R, Balliet JW, Gregory SA, Friedman H, Kolson DL, Nathanson N, Srinivasan A. 1992. An infectious molecular clone of an unusual macrophage-tropic and highly cytopathic strain of human immunodeficiency virus type 1. J Virol 66:7517–7521.
114. Kim FM, Kolson DL, Balliet JW, Srinivasan A, Collman RG. 1995. V3-independent determinants of macrophage tropism in a primary human immunodeficiency virus type 1 isolate. J Virol 69:1755–1761.
115. Doranz BJ, Rucker J, Yi Y, Smyth RJ, Samson M, Peiper SC, Parmentier M, Collman RG, Doms RW. 1996. A dual-tropic primary HIV-1 isolate that uses fusin and the beta-chemokine receptors CKR-5, CKR-3, and CKR-2b as fusion cofactors. Cell 85:1149–1158. https://doi.org/10.1016/s0092-8674(00)81314-8.
116. Bolger AM, Lohse M, Usadel B. 2014. Trimmomatic: a flexible trimmer for Illumina sequence data. Bioinformatics 30:2114–2120. https://doi.org/10.1093/bioinformatics/btu170.
117. Yates A, Akanni W, Amode MR, Barrell D, Billis K, Carvalho-Silva D, Cummins C, Clapham P, Fitzgerald S, Gil L, Giron CG, Gordon L, Hourlier T, Hunt SE, Janacek SH, Johnson N, Juettemann T, Keenan S, Lavidas I, Martin FJ, Maurel T, McLaren W, Murphy DN, Nag R, Nuhn M, Parker A, Patricio M, Pignatelli M, Rahtz M, Riat HS, Sheppard D, Taylor K, Thormann A, Vullo A, Wilder SP, Zadissa A, Birney E, Harrow J, Muffato M, Perry E, Ruffier M, Spudich G, Trevanion SJ, Cunningham F, Aken BL, Zerbino DR, Flicek P. 2016. Ensembl 2016. Nucleic Acids Res 44:D710–D716. https://doi.org/10.1093/nar/gkv1157.
118. Dobin A, Davis CA, Schlesinger F, Drenkow J, Zaleski C, Jha S, Batut P, Chaisson M, Gingeras TR. 2013. STAR: ultrafast universal RNA-seq aligner. Bioinformatics 29:15–21. https://doi.org/10.1093/bioinformatics/bts635.
119. Anders S, Pyl PT, Huber W. 2015. HTSeq—a Python framework to work with high-throughput sequencing data. Bioinformatics 31:166–169. https://doi.org/10.1093/bioinformatics/btu638.
120. Robinson MD, Oshlack A. 2010. A scaling normalization method for differential expression analysis of RNA-seq data. Genome Biol 11:R25. https://doi.org/10.1186/gb-2010-11-3-r25.
121. McCarthy DJ, Chen Y, Smyth GK. 2012. Differential expression analysis of multifactor RNA-Seq experiments with respect to biological variation. Nucleic Acids Res 40:4288–4297. https://doi.org/10.1093/nar/gks042.
122. Chen Y, Lun ATL, Smyth GK. 2014. Differential expression analysis of complex RNA-seq experiments using edgeR, p 51–74. *In* Datta S, Nettleton D (ed), Statistical analysis of next generation sequencing data. Frontiers in probability and the statisical sciences. Springer, Cham, Switzerland. https://doi.org/10.1007/978-3-319-07212-8_3.
123. Benjamini Y. 2010. Discovering the false discovery rate. J R Stat Soc Series B Stat Methodol 72:405–416. https://doi.org/10.1111/j.1467-9868.2010.00746.x.
124. Subramanian A, Tamayo P, Mootha VK, Mukherjee S, Ebert BL, Gillette MA, Paulovich A, Pomeroy SL, Golub TR, Lander ES, Mesirov JP. 2005. Gene set enrichment analysis: a knowledge-based approach for interpreting genome-wide expression profiles. Proc Natl Acad Sci U S A 102:15545–15550. https://doi.org/10.1073/pnas.0506580102.
125. Liberzon A, Birger C, Thorvaldsdottir H, Ghandi M, Mesirov JP, Tamayo P. 2015. The Molecular Signatures Database (MSigDB) hallmark gene set collection. Cell Syst 1:417–425. https://doi.org/10.1016/j.cels.2015.12.004.
126. Gundem G, Lopez-Bigas N. 2012. Sample-level enrichment analysis unravels shared stress phenotypes among multiple cancer types. Genome Med 4:28. https://doi.org/10.1186/gm327.